Received: 10 July 2018 | Revised: 14 January 2019 | Accepted: 7 March 2019

DOI: 10.1002/joc.6070

International Journal of Climatology RMetS

RESEARCH ARTICLE

Multifractal characterization of meteorological drought in India using detrended fluctuation analysis

S. Adarsh[1] | D. Nagesh Kumar[2] | B. Deepthi[1] | G. Gayathri[1] | S. S. Aswathy[1] | S. Bhagyasree[1]

[1]Department of Civil Engineering, TKM College of Engineering, Kollam, India

[2]Department of Civil Engineering, Indian Institute of Science, Bangalore, India

Correspondence
S. Adarsh, Department of Civil Engineering, TKM College of Engineering, Kollam 691005, India.
Email: adarsh.sankaran@yahoo.in

This study presents multifractal detrended fluctuation analysis (MF-DFA) to describe the multifractality of Standardized Precipitation Index (SPI) series from 30 meteorological subdivisions of India estimated at different aggregation timescales (3, 6 and 12 months) based on long-term monthly rainfall data sets of 1871–2016 period. The plots of fluctuation function and generalized Hurst exponents confirmed that multifractality is evident in most of the SPI series; however, it is found that its strength and persistency differ with timescale and space. The Hurst exponents of long-term (SPI-12) and medium-term (SPI-6) drought series of all subdivisions showed long-term persistence irrespective of the climatic conditions of the region, while the short-term droughts (SPI-3) of six subdivisions displayed short-term persistence. Further, the analysis by partitioning the data to four time spells: 1871–1905, 1906–1940, 1941–1975 and 1976–2016 showed that the persistency of long- and medium-term drought is rather permanent. The analysis on changes in multifractal properties with respect to the climatic shift of 1976/1977 period showed that there is a clear increase in multifractal properties of all types of drought series in the recent past (post-1976 period). This study also finds that the Hurst exponents and degree of multifractality of all types of droughts increase with increase in aggregation timescales. The multifractality of all the long-term drought series (SPI-12) and most of the SPI-6 series are found to be due to correlation properties, while that of SPI-3 is because of joint effect of correlation properties and the broadness of probability distribution.

KEYWORDS

climate shift, drought, multifractal, scale, SPI

1 | INTRODUCTION

The information of long/short-range power law correlations in hydro-meteorological variables such as rainfall, streamflow and drought indices is helpful in their improved simulation and forecasting. The efforts for estimation of such correlation structures perhaps started from the times of Hurst (1951). Hydrological time series often possesses multi-scaling behaviour and it may display self-similar and exhibit fractal behaviours over certain range of timescales and capturing such characteristics may help for commenting the long/short memory of hydrological time series. Mandelbrot (1974, 1982) contributed extensively in the scaling analysis by giving proper theoretical framework for performing such analysis. In the past, several researchers have applied different methods to describe the multifractal properties of geophysical time series, which includes the rescaled range (R/S) analysis (Hurst, 1951), double trace moments (Tessier *et al*., 1996), and Fourier spectral analysis (Hurst *et al*., 1965; Pandey *et al*., 1998), extended self similarity (ESS) principles (Dahlstedt and Jensen, 2005), multifractal detrended fluctuation analysis (MF-DFA; Kantelhardt *et al*., 2002) and wavelet analysis (Kantelhardt *et al*., 2003). Many studies in the past investigated the fractal behaviour of streamflow and

precipitation series employing the classical Fourier analysis (Tessier *et al*., 1996; Pandey *et al*., 1998).

Olsson and Niemczynowicz (1996) evaluated the multifractal behaviour of daily rainfall observations from a dense rain gage network in southern Sweden. The total rainfall process in the area as well as the data after grouping based on the rainfall generating mechanism (warm fronts, cold fronts, convection, etc.) were analysed for multifractality. Both analyses confirmed multifractality of daily rainfall and multifractal properties of the total rainfall process agreed well with the properties of the cold front group. The multifractal properties displayed distinct differences because of the physical differences of the rainfall generating mechanisms. Tessier *et al*. (1996) detected scaling regimes of daily rainfall and runoff from 30 catchments in France using the Fourier spectral analysis. A scale break roughly at 16 days, corresponding to the "synoptic maximum" was detected in both rainfall and runoff series. The universal multifractal model (UMM) parameters as well as the scaling exponents were estimated. Subsequently, the exponents were used for the simulation of the time series. The detrended fluctuation analysis (DFA) proposed by Peng *et al*. (1994) was reported to be an appropriate method to calculate the variance of data at different scales. Kantelhardt *et al*. (2002) extended DFA into its multifractal variant namely MF-DFA which enables the detection of multifractal behaviour of data. Owing to its simplicity and robustness the method became very popular for the fractal characterization of daily, monthly or annual streamflow and precipitation records from different parts of the world (Kantelhardt *et al*., 2003; 2006; Koscielny-Bunde *et al*., 2003; Zhang *et al*., 2008; 2009a; 2009b; Rego *et al*., 2013; Yu *et al*., 2014; Li *et al*., 2015; Tan and Gan, 2017). Kantelhardt *et al*. (2003) investigated the multifractal temporal scaling properties of river discharge and precipitation records from different parts of the globe at different temporal scales. The results of the MF-DFA method were compared with the results by wavelet transform modulus maxima (WTMM) technique and obtained reasonably good agreement. They reported a non-universal behaviour of fluctuation exponents and weaker, but significant multifractality in the precipitation records. They evaluated the suitability of different multifractal models and found that a modified version of the binomial multifractal model was sufficient for runoff records, while several precipitation records required different models. In one seminal work by Kantelhardt *et al*. (2006), the authors investigated the multifractal behaviour of 99 long-term daily precipitation records and 42 long-term daily runoff records from different parts of the world. They found that the precipitation records generally show short-term persistence and runoff records show long-term persistence (LTP) with a mean scaling exponent of ~0.73 for runoff records globally. Further, for the multifractal characterization of the data, the generalized Hurst exponents (GHEs) were determined and fitted by three candidate operational models. The fits based on UMM described well the scaling behaviour of the positive moments in most of the runoff and precipitation records. For some precipitation records with weak multifractality, a simple bifractal characterization had given the best fit of the data. The modified version of the multiplicative cascade model was found to be suitable for all runoff records and most of the precipitation records, for the scaling behaviour of both positive and negative moments.

Yu *et al*. (2014) evaluated the multifractal properties of daily rainfall time series at the stations in Pearl River basin of China over periods of up to 45 years. They used universal multifractal approach based on the multiplicative cascade model and the MF-DFA. The results by both the approaches confirmed the multifractality, but in two different timescale ranges and the MF-DFA indicated short-term correlations for the data sets. The study also investigated the relationship between topography and rainfall variability and found that rainfall and elevation series are negatively correlated. Baranowski *et al*. (2015) characterized the scaling properties of 11,322 measured time series (of 31 year duration) of daily air temperature, wind velocity, relative air humidity, global radiation and precipitation from stations located in Finland, Germany, Poland and Spain. For most of the series, multifractality was found be due to long range correlations, while that for the precipitation was found to be due to broadness of probability distribution. Tan and Gan (2017) used MF-DFA for detecting LTP and multifractal behaviour of 100 stations of daily precipitation and 145 stations of streamflow time series of Canada. They reported that all precipitation time series showed LTP at both small- and large-timescales, while streamflow time series generally showed non-stationary behaviour at small timescales and LTP at large timescales. The multifractal behaviour of Canadian precipitation and streamflow data could be accurately described by the UMM and with the modified version of multiplicative cascade model. They suggested that the persistence of Canadian streamflow was not only because streamflow is more autocorrelated than precipitation but also due to human interventions such as streamflow regulations.

The hydrological extremes such as drought have direct and significant implications on the water resources and agricultural productivity of a region. For the prediction, monitoring, and assessment of droughts, several drought indices have been proposed over the years based on primary factors leading to drought such as precipitation, evapotranspiration, vegetation conditions, etc. (Zargar *et al*., 2011). The Rainfall Anomaly Index (RAI; Van-Rooy, 1965), Palmer Drought Severity Index (PDSI; Palmer, 1965), Standardized Precipitation Index (SPI; McKee *et al*., 1993) and Standardized Precipitation Evapotranspiration Index (SPEI; Vicente-Serrano *et al*., 2010) are some among them. SPI perhaps is the most popular drought index owing to the flexibility of timescale, the requirement of fewer input variables, and

ease in estimation (Bazrafshan *et al*., 2013). In recent past, few studies focused on variability of droughts in different parts of India and for the whole India using SPI as drought index (Pai *et al*., 2011; Ganguli and Janga Reddy, 2013; Thomas *et al*., 2015; Joshi *et al*., 2016; Thomas and Prasannakumar, 2016). As the drought indices are quantified based on hydro-meteorological variables like precipitation, evapotranspiration and streamflow, it is logical to suspect fractal properties in such derived indices also. However, the multifractal analysis of hydrological extremes like floods or droughts is really scarce in literature while in the past decade, few studies in this direction were reported (Hou *et al*., 2015; 2017; Zhang *et al*., 2016). Tatli (2015) determined persistence in the PDSI of 1966–2010 period over Turkey by determination of scaling (Hurst, H) exponent using classical rescaled range analysis, but did not estimate other multifractal properties of the series. The author computed the parameters such as predictability index, fractal dimension and autocorrelation function of the PDSI values from the estimated Hurst exponents. Subsequently, the Mann–Kendall (MK) test was used to determine the trend of PDSI series. The results showed that significant negative trends were widespread throughout the country and it was found that *H* values were close to 1 in places where statistically significant trends exist. The high values of the Hurst exponent in all the regions were attributed to the possible association between drought and the large-scale atmospheric circulations. Hou *et al*. (2017) performed multifractal characterization of drought from seven regions in China considering the SPI series, based on monthly rainfall data of 1961–2012 period. The SPI series of North and North West regions of China showed short-term persistency while in the remaining regions, the SPI showed LTP. The multifractality was found to be the highest in south eastern region, where the drought prediction was most difficult, and they provided some arguments on physical mechanism of the rainfall pattern of the study area to explain the multifractal behaviour of drought index.

According to the authors' knowledge, none of the studies in the past attempted the investigation on the changes in the multifractality with change in aggregation timescale and the temporal variability of multifractal properties of drought index series. Moreover, in the Indian context no studies on multifractal analysis of drought index are reported. In short, a comprehensive multifractal analysis of drought indices is still an open research problem in general and in the Indian context in particular. Thus, the specific objectives of this paper are framed as: (a) to perform multifractal analysis of SPI series of different meteorological subdivisions in India; (b) to investigate the changes in multifractal characteristics of SPI series of different aggregation timescales; (c) to investigate the temporal sensitivity of multifractal characteristics of SPI series considering different time spells of rainfall data of last century.

2 | MATERIALS AND METHODS

In the following section, a brief description on the MF-DFA algorithm is provided:

2.1 | Multifractal detrended fluctuation analysis

The MF-DFA can be used to detect the scaling behaviours and multifractal properties of non-stationary time series such as hydrological series. The different steps involved in MF-DFA procedure can be described as follows (Kantelhardt *et al*., 2002; Zhang *et al*., 2009a; Li *et al*., 2015).

1. Consider a time series X (x_1, x_2, …, x_N) where N is the length of the time series. The accumulated deviation of the series (known as "profile") is calculated as

$$Y(i)=\sum_{k=1}^{i}[x_k-\bar{x}], \tag{1}$$

where $i = 1, 2, \ldots, N$, $k = 1, 2, \ldots, N$, $\bar{x}$ is the mean of the series x_k.

2. Divide the profile $Y(i)$ into $N_s = \text{int}(N/s)$ non-overlapping segments of length, where s is the segment sample size (popularly called as scale) chosen for the analysis and int(N/s) is the integer part of (N/s). While considering multiple timescales, sometimes a small portion of the time series at the end may be left out, as N need not be a multiple of s always. To retain this part of the series, the same procedure is repeated starting from the opposite end resulting in $2N_s$ segments.
3. Calculate the local trend for each of the $2N_s$ segments by least squares fit of the series as

$$F^2(s,\nu)=\frac{1}{s}\sum_{i=1}^{s}\{Y[(\nu-1)s+i]-y_\nu(i)\}^2 \text{ for } \nu=1,2,\ldots N_S, \tag{2}$$

$$F^2(s,\nu)=\frac{1}{s}\sum_{i=1}^{s}\{Y[N-(\nu-N_s)s+i]-y_\nu(i)\}^2 \text{ for } \nu=N_S+1,\ldots,2N_S. \tag{3}$$

Here $y_\nu(i)$ is the fitting polynomial in segment ν. Different types of fittings such as linear, quadratic, cubic, etc. can be made and accordingly DFA procedure is named as DFA1, DFA2,…, DFAm, etc.

4. Determine the qth-order fluctuation function by averaging over all segments

$$F_q(s) = \left\{ \frac{1}{2N_s} \sum_{\nu=1}^{2N_s} \left[F^2(s,\nu) \right]^{q/2} \right\}^{1/q}. \quad (4)$$

Here the index variable q can take any real value except zero.

For the zeroth order, the fluctuation function can be computed by following a logarithmic averaging procedure defined in Kantelhardt *et al*. (2002):

$$F_0(s) = \exp\left\{ \frac{1}{4N_s} \sum_{\nu=1}^{2Ns} \ln \left[F^2(s,\nu) \right] \right\}. \quad (5)$$

5. Determine the scaling behaviour of the fluctuation functions by analysing the log–log plots of $F_q(s)$ versus s for each value of q. If the time series is long range power law correlated, $F_q(s)$ increases as $F_q(s) \sim s^{h(q)}$ where $h(q)$ is the GHE.

For each order of q, the scaling behaviour of the fluctuation functions can be determined by the logarithmic plot of $F_q(s)$ versus s. The slope of log $F_q(s)$ and log (s) plot is the GHE $h(q)$. For stationary time series, $0 < h\ (q = 2) < 1$, is identical to the classical Hurst exponent (Hurst, 1951). For non-stationary time series, $h(q = 2) > 1$ and the relation between $h(2)$ and H can be given as $H = h(2) - 1$ (Zhang *et al*., 2009a). For an uncorrelated series the value of Hurst exponent is 0.5. If the Hurst exponent falls between 0.5 and 1, it indicates the LTP (long memory process) and if it falls between 0 and 0.5, it indicates a short-term persistence (short memory process). LTP implies a positive auto correlation in the time series (i.e., the effect of an observation on future observations remain significant for a long period of time), for example if an extreme event would have higher probability being followed by another extreme of same character (i.e., a flood followed by another flood). The selection of scale (s), the type of polynomial chosen etc. are some of the major issues in applying the MF-DFA method. Generally sufficient segments are chosen between the bounds (minimum and maximum) scale range. Minimum scale can be chosen in such a way that it is sufficiently larger than the polynomial order chosen to prevent error in computation of local fluctuations. Maximum scale below half of the data length can be chosen. The maximum segment size should be small enough to provide a sufficient number of segments in the computation of fluctuation function. Also, the polynomial order from 1–3 would probably be sufficient to avoid overfitting problem within small segment sizes (Ihlen, 2012). In this study, a polynomial order of 1 is chosen and the plots between scale and fluctuation function for $q = 2$ (in log scale) are prepared by considering the maximum scale as half of the data length (Hajian and Movahed, 2010).

The description of different derived multifractal parameters and their physical significance are provided in Appendix.

2.2 | Standardized Precipitation Index

SPI is a measure which has been used widely to identify droughts of different types such as agricultural, meteorological, etc. The SPI series can be prepared by considering different aggregation timescales such as 1, 3, 6, 12, 24 and 48 months. The 3-month SPI (SPI-3) can be used as a seasonal drought index to represent short-term drought, the 6-month SPI (SPI-6) for intermediate term and the 12-, 24- and 48-month SPI for long-term drought (Thomas *et al*., 2015). As SPI of different timescales can indicate short-term as well as long-term droughts, the results have significant implications on different components of hydrologic cycle. Soil moisture may be more sensitive to a 3-month SPI representing the water stress and crop failures, while streamflow drought conditions may be reflected by the 6-month SPI, and the groundwater drought conditions may be better represented by the 12- and 24-month SPI values (Thomas *et al*., 2015).

The computation of SPI involves the following steps:

1. Preparation of aggregated precipitation series for specified accumulation timescale (say 3, 6, 12 months, etc.).
2. Fitting of Gamma distribution function on this series. The cumulative distribution function (CDF) is computed as $F_x(x) = q + (1 - q)G_x(x)$ to account for the zero values, as the two parameter Gamma distribution is not defined for zero precipitation values, where q is the probability of zero precipitation in historical records; $G_x(x)$ is the CDF of non-zero precipitation records and $F_x(x)$ is the CDF of actual precipitation series.
3. Performing an equi-probability transformation between CDF of mixed distribution and standard normal distribution, to get the SPI for given timescale, that is, $Z = \psi^{-1}(F_x(x))$, where $\psi^{-1}(\cdot)$ is the inverse of the CDF.

3 | STUDY AREAS AND DATA SETS

Indian Institute of Tropical Meteorology (IITM) Pune classified India into 36 meteorological subdivisions based on rainfall homogeneity. A map showing the different meteorological subdivisions is presented in Figure S1, Supporting Information. The database was prepared initially by Parthasarathy *et al*. (1995) with an available network of 306 stations. Missing data for individual stations was filled up by the rainfall data of a neighbouring rain gauge station by following standard procedures. As a first step in data preparation, the district-wise monthly rainfall was calculated as the arithmetic average of rainfall data of all the stations in the district. Then monthly area weighted rainfall of the subdivisions was prepared by assigning district area as the weight for different rain gauge stations. Before releasing the data, the IITM and India Meteorological Department (IMD) perform a rigorous quality check and thus the data forms as

one of the most reliable long-time series data available for the research community. The database was updated periodically (Guhathakurta and Rajeevan, 2008; Guhathakurta *et al*., 2015) as joint venture of IITM and IMD and the latest version (Kothawale and Rajeevan, 2017) is used in the present study. IITM prepared the recent versions of subdivisional rainfall data by using observational data from a network of 1,476 meteorological stations (by maintaining at least one representative station per district). The monthly area weighted precipitation data of these subdivisions for the period 1871–2016 are available at http://www.tropmet.res.in/, which can be used for estimation of drought index (i.e., SPI) at different aggregation timescales. In the present study, the multifractal properties of meteorological drought index SPI of 30 subdivisions for which the rainfall data is available are estimated. To demonstrate the results, first the multifractal properties of SPI series of four meteorological subdivisions—western Rajasthan (WR), Saurashtra, Kutch and Diu (SKD), Marathwada (MW) and Kerala (KER) are considered. The first three subdivisions are falling in arid/semi-arid zones of India and have history of frequent droughts. These three subdivisions are particularly considered by other researchers in meteorological drought studies (Ganguli and Janga Reddy, 2013). Kerala, located in the southwestern coast of India, is one of the high rainfall-receiving regions (average annual rainfall of ~300 cm) which is known as "gateway of Indian monsoon." Hence, the region is having distinctly different climatological conditions, in comparison with other three subdivisions. Many studies reported a reduction in rainfall and consequent signature of droughts, in the state of Kerala (Krishnakumar *et al*., 2009; Adarsh and Janga Reddy, 2015; Thomas and Prasannakumar, 2016; Adarsh *et al*., 2018). In order to investigate the similarity or differences in the multifractal behaviour of the spatially aggregated data and individual station data, the monthly data of 50 stations (for 1983–2016 period) in Kerala operated by IMD is used.

4 | RESULTS AND DISCUSSION

In this section, the results of different analyses and corresponding discussions are provided.

4.1 | Multifractal characteristic analysis of drought

The monthly rainfall time series from different subdivisions are used for estimating the SPI time series of timescales 3, 6 and 12 months. The multifractalities of different SPI series are investigated systematically by plotting the relationships between fluctuation function and segment sample size ($F_q(s)$ vs. s) and determine the GHE for the selected moment order ($h(q)$ vs. q). The fluctuation function (F_q) was obtained for each value of order q from −5 to 5. The different slopes of fluctuation function (F_q) plot for different moment orders (q) are an evidence of multifractality of the series and these slopes are known as GHE ($h(q)$). Subsequently, the GHEs ($h(q)$) are plotted against moment order q and its nonlinear dependency is also an indicative of multifractality of the series. Similar plots have been obtained for all the subdivisions. The plots of fluctuation function against scale of four typical subdivisions of WR, Saurashtra–Kutch–Diu (SKD), MW and KER for different SPI series are provided in Figure 1.

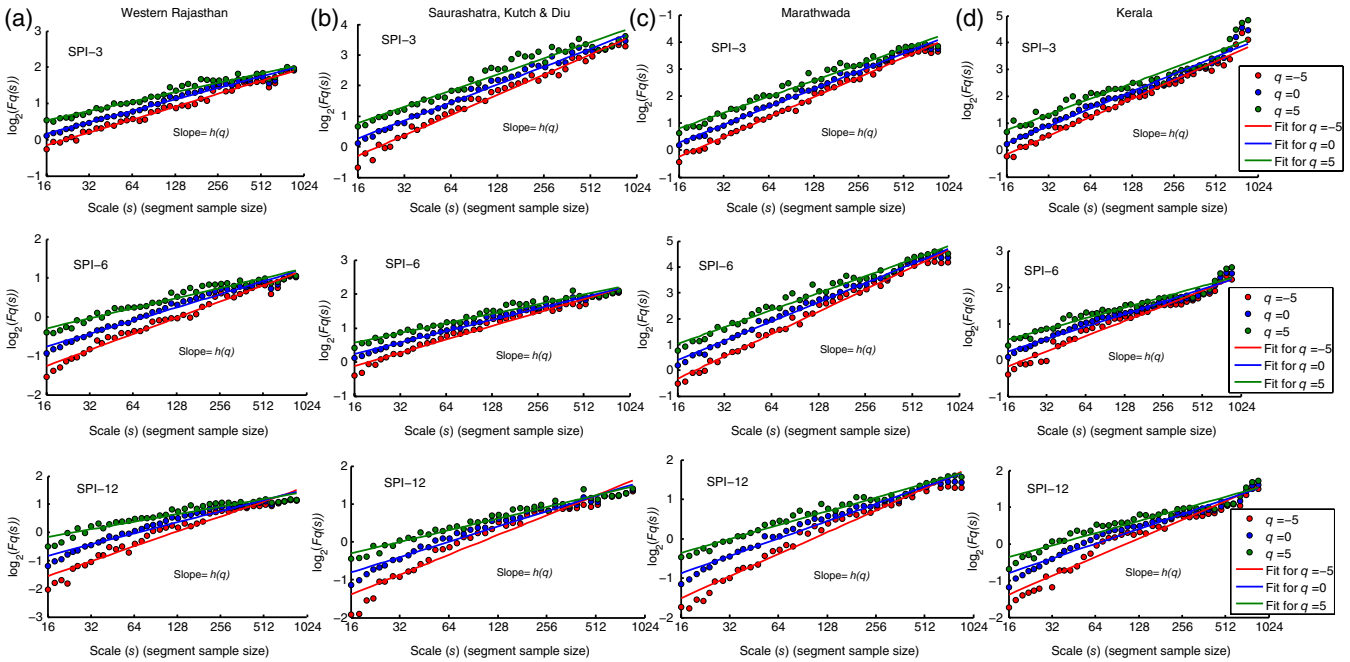

FIGURE 1 Plots of fluctuation function depicting multifractality of SPI series of four subdivisions. The first column show the plots of SPI series of WR and remaining columns show the results of SK. MW and KER subdivisions. The first, second and third rows row show the results of SPI-3, SPI-6 and SPI-12 series of different subdivisions [Colour figure can be viewed at wileyonlinelibrary.com]

Figure 1 shows that all the 12 time series possess multifractality, as the slopes of the plots of fluctuation function with segment sample size for different moment orders are different. Further, the plots of $h(q)$ vs. q of different SPI series of the four subdivisions are provided in Figure 2. In this study, q value is varied from −5 to 5 with small intervals of 0.25 for capturing the variation in a detailed way. The q-dependency of $h(q)$ clearly depicts the multifractality of the SPI time series, even though their strengths differ. The same conclusion holds good for SPI series of the remaining 26 subdivisions as well. For negative q value, the $h(q)$ value is increasing which indicates the scaling behaviour of segments with small fluctuations, where as for positive q value, $h(q)$ value is decreasing which indicates the scaling behaviour of segments with large fluctuations. The value of GHE at moment order 2 (i.e., $h(q)$ for $q = 2$) is denoted as Hurst exponent (H) of the series (Kantelhardt *et al*., 2006). The value of H is indicative of short/long memory of the time series which can be linked with the autocorrelation structure of the series (Bassingthwaighte and Beyer, 1991; Bassingthwaighte and Raymond, 1995). The difference between $h(q\text{min})$ and $h(q\text{max})$ (in this case, $q$min and $q$max are −5 and 5, respectively) helps to compare the degree of multifractality of different series. Higher the value of total spread of GHE plot (Δh), greater will be the degree of multifractality. The total spread (Δh), Hurst exponent (H) value, left and right spread (Δh_L and Δh_R), of the four subdivisions are summarized in Table 1.

In the different cases of the four subdivisions considered first, the Hurst exponent values vary between 0.5 and 1, which indicates the LTP (long memory dependency structure) of different SPI series. The variation of values of Hurst exponent is dependent on the scale and over the subdivisions. For an aggregation timescale of 3, the variation is from 0.55 to 0.62 and for a scale of 6 the variation is from 0.6 to 0.7, whereas, for timescale of 12 the variation ranges from 0.67 to 0.79 considering the four subdivisions. Among the three SPI series, the highest value of Hurst exponent is noticed for MW subdivision. Figure 2 shows that SPI-3 series of different subdivisions posses the least variation of $h(q)$, while SPI-12 series possess large variation. This indicates that multifractal degree increases with increase in aggregation timescale.

An in-depth multifractal characteristic analyses of different SPI time series are made in different ways, the mass exponent plot ($\tau(q)$ vs. q) and the multifractal spectra in particular. The difference in slopes of the different segments gives information on the degree of multifractality of the time series. There are different behaviours for $q < 0$ and $q > 0$ of the mass exponent plots. The nonlinear $\tau(q)$ means multiple scaling, and the degree of nonlinearity of the $\tau(q)$ function reflects the degree of multifractality. The mass exponent plots of SPI-3, SPI-6 and SPI-12 series of the four subdivisions are presented in Figure 3. Slopes corresponding to $q < 0$ and $q > 0$ are obtained by linear fitting. The plots show that the behaviour is different for $q < 0$ and $q > 0$ and possess different slopes before and after the value for $q = 0$, which are marked in the respective panels. The slopes indicated in Figure 3 show that the difference in the slopes of the two segments of WR subdivision are 0.193, 0.324 and 0.554 for time series of SPI-3, SPI-6 and SPI-12. The differences in the slopes of the SPI series of SK subdivision are 0.14, 0.239 and 0.456; those of MW subdivision are 0.152, 0.220 and 0.436 and for the KER subdivision the values are respectively 0.115, 0.254 and 0.381. The numerical difference in slopes of the segments indicates that highest multifractal degree is noticed in the SPI-12 of WR subdivision. This analysis also confirms that multifractal degree of drought increases with increase in aggregation timescale.

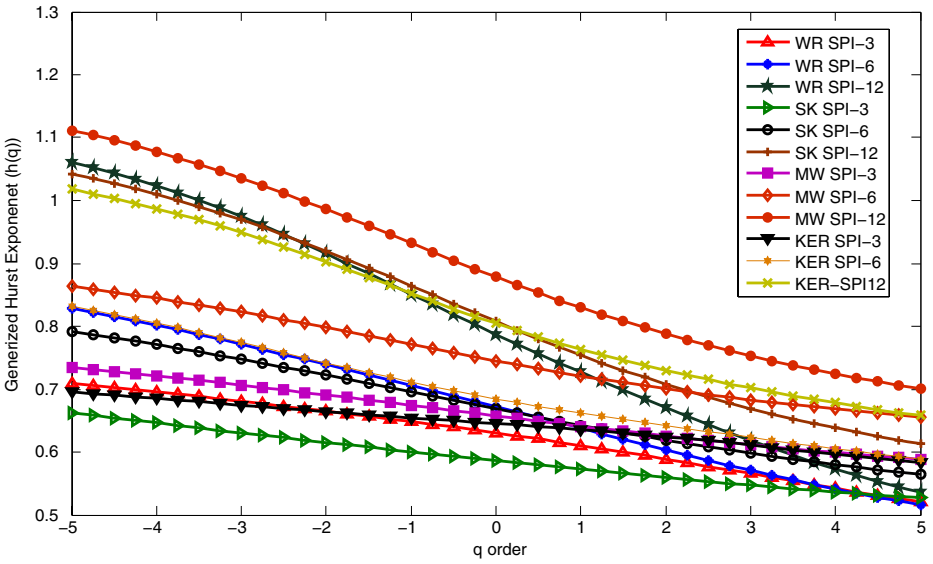

FIGURE 2 GHE plots of SPI series of four subdivisions [Colour figure can be viewed at wileyonlinelibrary.com]

TABLE 1 Parameters of GHE plots of SPI 3, 6 and 12 time series of four subdivisions

	SPI-3				SPI-6				SPI-12			
Subdivision	$\Delta h(q)_L$	$\Delta h(q)_R$	$\Delta h(q)$	**H**	$\Delta h(q)_L$	$\Delta h(q)_R$	$\Delta h(q)$	**H**	$\Delta h(q)_L$	$\Delta h(q)_R$	$\Delta h(q)$	**H**
WR	0.079	0.110	0.189	0.589	0.155	0.156	0.311	0.604	0.273	0.251	0.524	0.671
SKD	0.076	0.059	0.135	0.559	0.123	0.104	0.227	0.619	0.235	0.194	0.429	0.708
MW	0.076	0.069	0.146	0.626	0.118	0.089	0.207	0.700	0.233	0.178	0.411	0.788
KER	0.050	0.063	0.113	0.624	0.147	0.096	0.243	0.642	0.214	0.146	0.360	0.730

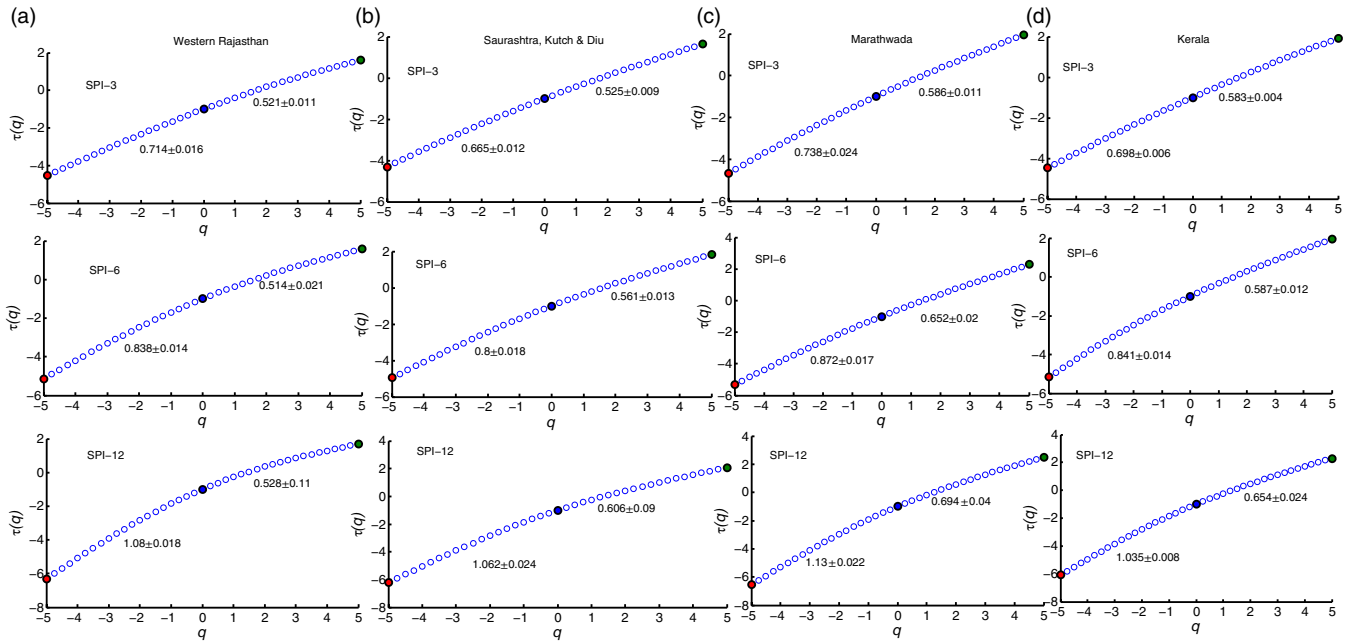

FIGURE 3 Plot of mass exponent with moment order ($\tau(q)$ vs. q) of different SPI series (SPI-3, SPI-6 and SPI-12) of different subdivisions (a) WR; (b) SK; (c) MW; (d) KER. The slopes of the segments are given in the respective figures [Colour figure can be viewed at wileyonlinelibrary.com]

Next, the multifractal spectra of SPI series of different subdivisions are determined, and their properties are analysed in detail. Apart from the base width of the spectra (α), width of left and right branches ($\Delta\alpha_L$ and $\Delta\alpha_R$) and asymmetric index (R) are also computed for each case. For illustration, the multifractal spectrum of SPI series of four subdivisions for 1871–2016 period are presented in Figure 4. For a multifractal time series, the shape of singularity spectrum will be an inverted parabola whose left and right-hand limbs correspond to positive and negative q, respectively, and the spectra will converge to a point for a mono-fractal series. Different panels of Figure 4 show that different multifractal spectra exhibit parabolic shape indicating the multifractal structure of the time series. On examining the plots, it can be noted that the spectra of SPI-6 and SPI-12 are close to symmetrical, while many of the multifractal spectra are found to be unsymmetrical. This indicates that the long-term droughts of different subdivisions are more stable. The long right tail of the spectra indicates that multifractal structure of the time series is insensitive to large magnitudes of local fluctuations, while the long left tails indicate that the series is insensitive to local fluctuations of small magnitudes (Ihlen, 2012). The values of the parameters of multifractal spectra of different series pertaining to the four subdivisions are summarized in Table 2.

The ranges of base width of multifractal spectra ($\alpha_{\max} - \alpha_{\min}$) of SPI-3 series are 0.22–0.35 (marked in the respective figures) in different subdivisions. The values range between 0.34 and 0.54 for the SPI-6 series while the range is 0.58–0.84 for the SPI-12 series of different subdivisions. The base width of multifractal spectra is quantified, which is a measure of multifractal degree of the time series. On considering a specific subdivision, the multifractal degree increases with increase in aggregation timescale. For example, for WR subdivision, the widths of the spectra are 0.350, 0.54 and 0.842, respectively, for SPI-3, SPI-6 and SPI-12 series. On considering the overall climatology of these four subdivisions, the average annual rainfall based on data set of 1871–2016 period are ~29.9, 47.8, 82.8 and 282 cm, respectively, for WR, SK, MW and KER. This clearly indicates that the climatology shows distinct differences, for Kerala in particular. Irrespective of these climatological differences, the degree of multifractality increases with increase in aggregation timescale. Highest multifractal degree is noticed for the SPI series of WR subdivision while the lowest multifractal degree is noticed for KER subdivision for SPI-3 and SPI-12 series; but for moderate drought,

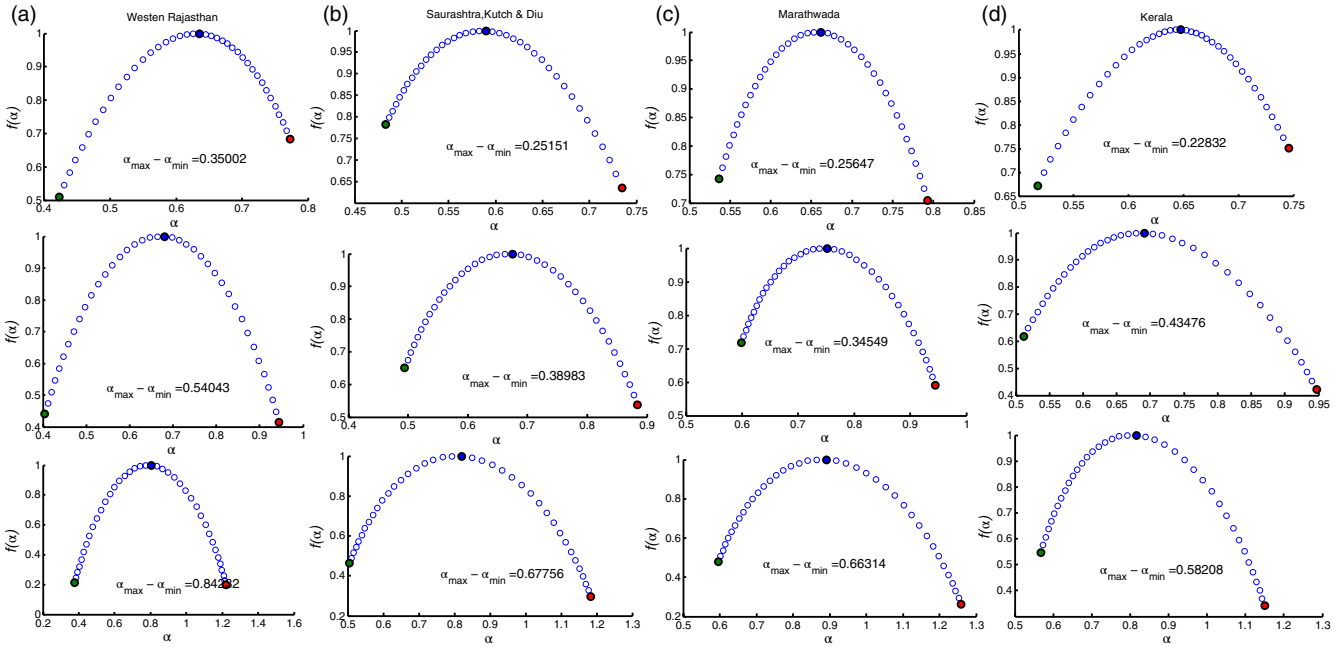

FIGURE 4 Multifractal spectra of SPI series of different subdivisions (a) WR; (b) SK; (c) MW; (d) KER. The upper panel shows the plots for SPI-3 series, middle panels shows the plots for SPI-6 series and lower panels shows the plots for SPI-12 series. The base width of the multifractal spectra are given in the respective panel [Colour figure can be viewed at wileyonlinelibrary.com]

the lowest multifractal degree was found to be for SPI-6 of MW subdivision. It is worth mentioning that the SPI series for the above subdivisions were computed based on the spatially averaged precipitation data for homogeneous regions. In order to ascertain its reliability, the station-wise data of the Kerala meteorological subdivision is considered. Even though 68 stations are operative from IMD, we considered the data of 50 stations, for which long and reliable data are available for the estimation of SPI. The multifractal properties like GHE, H, spectral width, asymmetric index (R), $\Delta f(\alpha)$ and α_0 of the station-wise data are determined. The spatial distribution of these properties is presented in Figure 5. The careful examination of the properties reveals that for the SPI derived from station data also, the multifractal strength and Hurst exponent increases with increase in aggregation timescale, but there is no uniform pattern of the properties with hilly, middle or coastal terrains of the subdivision. The precipitation of the state is mainly orographic in nature and Indian monsoon arrives the Kerala coast first in the first week of June and the changes in onset of the Indian monsoon influence the pattern of seasonal precipitation all over the country. Unlike many other parts of the country, the precipitation of the state of Kerala have two possible spikes as in addition to the summer monsoon (southwest monsoon), the post-monsoon (northeast monsoon) also contributes well to the precipitation of the state. Despite these inferences, the local factors may be playing a dominant role on precipitation of the state over the global processes of climate dynamics and it will be difficult to find a common reason how the exponents change with latitude, altitude or distance from the coast (Orun and Kocak, 2009).

4.2 | Spatiotemporal variability of multifractal parameters

In order to capture the spatial variability of multifractal parameters, the analysis is extended to all the remaining subdivisions of India. Further, by partitioning the data sets into four segments (1871–1905), 1906–1940, 1941–1975 and 1976–2016, similar exercise is performed, to capture the temporal variability of these parameters. The spatial distribution of the spread of GHE ($\Delta h(q)$) and Hurst exponent values of different SPI series of all the meteorological subdivisions for different time spells are presented in Figures 6 and 7, respectively. The Hurst exponent values of the SPI series of all subdivisions for different time spells are summarized in Table 3.

By examining the fluctuation function plots and the values of $\Delta h(q)$ and the base width of the spectra, it is noticed that the Δh values of these parameters are very less for SPI-3 series of Gangetic West Bengal, Orissa, Chattisgarh, Jharkhand and Vidarbha subdivisions, which indicates more or less homogenous precipitation in these areas. For monofractal series, the width of the spectrum will be zero (spectrum converge to a point) and $h(q)$ will be independent of q (Burgueño *et al*., 2014). This is an evidence of possible monofractality of the SPI-3 series of the above meteorological subdivisions with a systematic and marginal reduction of $h(q)$ with the moment order q. A considerable higher value of Δh in the regions like Tamilnadu and Sub-Himalaya indicates considerable heterogeneity in the precipitation in these areas. The results show that the degree of multifractality is highest for long-term drought (SPI-12) followed by SPI-6 and SPI-3.

TABLE 2 Hurst exponent values of SPI series of different subdivisions

	SPI-3					SPI-6					SPI-12				
Subdivision	**T**	**S1**	**S2**	**S3**	**S4**	**T**	**S1**	**S2**	**S3**	**S4**	**T**	**S1**	**S2**	**S3**	**S4**
Jharkhand	**0.498**	**0.429**	**0.351**	0.577	0.506	0.563	0.525	0.443	0.686	0.569	0.680	0.716	0.664	0.885	0.776
Kerala	0.624	0.55	0.525	0.659	0.572	0.642	0.601	0.636	0.792	0.725	0.730	0.725	0.785	1.032	0.929
Bihar	**0.490**	0.618	0.531	0.563	0.536	0.564	0.689	0.628	0.651	0.718	0.667	0.806	0.828	0.805	0.959
Tamilnadu	**0.454**	**0.428**	0.507	0.562	0.542	0.520	0.531	0.638	0.658	0.679	0.665	0.749	0.944	0.851	0.929
Vidarbha	0.617	0.63	0.631	0.673	0.512	0.679	0.724	0.694	0.721	0.581	0.779	0.862	0.881	0.870	0.686
East Rajasthan	0.561	0.607	**0.413**	0.654	0.627	0.627	0.673	0.500	0.740	0.727	0.763	0.829	0.700	0.944	1.009
Chattisgarh	0.615	0.529	0.548	0.697	0.614	0.678	0.638	0.665	0.772	0.648	0.778	0.828	0.857	0.888	0.752
Coastal Karnataka	0.515	0.540	0.591	0.677	0.573	0.529	0.587	0.650	0.720	0.637	0.597	0.677	0.740	0.900	0.832
MW	0.626	0.668	0.766	0.652	0.530	0.700	0.753	0.832	0.749	0.677	0.788	0.884	0.998	0.911	0.884
Telangana	0.544	0.736	0.761	0.514	**0.499**	0.595	0.830	0.782	0.590	0.590	0.711	0.966	0.933	0.798	0.743
Gujarat	0.559	0.611	**0.448**	0.668	0.654	0.619	0.726	0.524	0.703	0.687	0.718	0.886	0.677	0.824	0.885
West Rajasthan	0.589	0.775	0.519	0.579	0.711	0.604	0.814	0.621	0.664	0.777	0.671	0.916	0.831	0.830	0.942
North Karnataka	0.610	0.582	0.663	0.548	0.660	0.684	0.655	0.746	0.609	0.813	0.782	0.765	0.951	0.792	1.010
East Uttar Pradesh	0.570	0.515	0.556	0.606	0.502	0.631	0.606	0.647	0.690	0.607	0.739	0.845	0.908	0.883	0.823
Haryana & Delhi	0.520	0.633	0.548	**0.436**	0.548	0.579	0.711	0.639	**0.455**	0.612	0.739	0.929	0.829	0.559	0.786
Orissa	0.512	**0.482**	**0.420**	0.547	0.572	0.610	0.637	**0.484**	0.642	0.696	0.751	0.870	0.663	0.827	0.898
Coastal Andhra Pradesh	0.504	0.572	0.661	0.514	0.522	0.560	0.681	0.751	0.599	0.636	0.679	0.830	0.981	0.755	0.802
Nagaland	0.575	0.670	0.549	0.519	0.693	0.640	0.769	0.600	0.665	0.789	0.758	0.918	0.739	0.879	0.974
South Karnataka	0.526	0.639	0.522	0.544	0.684	0.606	0.725	0.612	0.609	0.832	0.700	0.873	0.781	0.705	0.961
Rayalaseema	**0.461**	0.551	0.543	0.525	0.548	0.509	0.622	0.592	0.524	0.639	0.617	0.731	0.758	0.720	0.783
West Madya Pradesh	0.610	0.564	0.561	0.757	0.613	0.686	0.592	0.606	0.847	0.710	0.803	0.782	0.777	1.028	0.899
East Madhya Pradesh	0.573	0.585	0.550	0.743	0.553	0.634	0.662	0.628	0.827	0.598	0.733	0.855	0.812	0.940	0.709
Punjab	0.500	0.597	0.559	0.359	0.507	0.571	0.656	0.654	0.459	0.580	0.719	0.789	0.851	0.649	0.758
Assam–Meghalaya	0.622	0.539	0.646	0.560	0.669	0.689	0.643	0.669	0.691	0.718	0.788	0.854	0.804	0.862	0.834
Konkan & Goa	0.626	**0.441**	0.712	0.583	0.595	0.692	0.556	0.773	0.704	0.702	0.769	0.690	0.924	0.898	0.843
West Uttar Pradesh	0.570	0.515	0.556	0.606	0.502	0.631	0.606	0.647	0.69	0.607	0.739	0.845	0.908	0.883	0.823
Gangetic West Bengal	0.567	0.541	0.562	0.571	**0.458**	0.612	0.616	0.635	0.665	0.566	0.704	0.821	0.782	0.847	0.718
Sub-Himalaya	0.541	0.524	**0.466**	**0.346**	0.629	0.599	0.581	0.569	**0.468**	0.836	0.700	0.730	0.809	0.716	1.045
Madhya Maharashtra	0.629	0.629	0.649	0.735	0.566	0.690	0.697	0.746	0.787	0.726	0.771	0.800	0.951	0.935	0.932
SKD	0.559	0.559	**0.467**	0.571	0.812	0.619	0.673	0.556	0.608	0.851	0.708	0.847	0.746	0.725	0.972

Note. T = total time spell (1871–2016); S1 = 1871–1905; S2 = 1906–1940; S3 = 1941–1975; S4 = 1976–2016 period. The values in bold infer that the Hurst exponent less than 0.5 indicating a short-term persistence.

From Table 3, it can be noted that the Hurst exponent value increases with the increase in aggregation timescale for all cases. It is further noticed that SPI-3 of Jharkhand, Tamilnadu, Rayalaseema and Bihar show short-term power law correlation (values in italics, ruling out those close to 0.5). It is also noted that except for one of the time spells, the persistency of SPI-3 of Jharkhand is short term. This information of short memory is informative in modelling of short-term drought, while it is to be noted that the time spell under consideration may slightly influence the values. In general, the short-term persistency is seen mainly for an aggregation timescale of 3, that is, the short-term drought of India is more liable to display the character of short-term persistency. The long-term persistency of SPI-12 is rather permanent, as none of the time spells and none of the series show short-term power law correlation. In SPI-6 also, only in certain localized time spells the short-term persistency structure exists, while in most of the time spells, the persistency is long-term. That means, for higher aggregation timescales the persistency is also high. In short, the forthcoming predictions of drought are strongly governed by trends on the preceding drought. Due to the long-term power law correlations in the time series, large values are rather followed by large values and small values are rather followed by small values, leading to periods with fewer drought events. From the fluctuation function and GHE plots, it can be noted that SPI series of all the subdivisions exhibit multifractality.

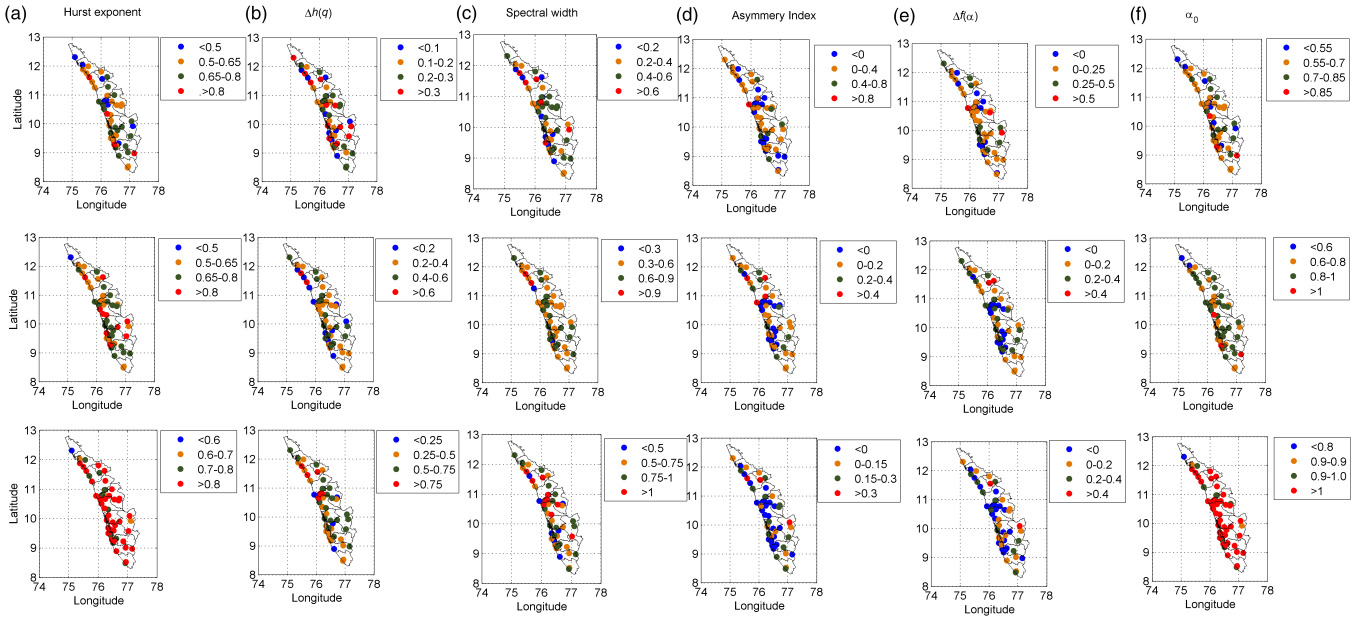

FIGURE 5 Distribution of parameters of the GHE plot and that of multifractal spectra of Kerala subdivision. (a) Hurst exponent; (b) $\Delta h(q)$; (c) spectral width; (d) asymmetry index; (e) $\Delta f(\alpha)$; (f) α_0. Upper panels show the results of SPI-3 series; middle panels show the results of SPI-6 series and lower panels show the results of SPI-12 series [Colour figure can be viewed at wileyonlinelibrary.com]

Next, multifractal spectrums are developed for all the three SPI series of all the subdivisions and the spatial distribution of different characteristic properties of the spectra are analysed. The spatial distribution of multifractal spectral width is presented in Figure 8. There is variation in the width of multifractal spectrum over subdivisions and aggregation timescales. The value of width of singularity spectrum ranges from 0.16 to 0.43 for timescale 3; from 0.25 to 0.55 for timescale 6 and from 0.45 to 0.84 for timescale 12 for 1871–2016 series. Thus, it is clear that the width increases with increase in aggregation timescale which is also found to be true for other time spells. From our study it was found that, in all cases, the multifractal spectra are continuous and asymmetrical convex parabolas, which indicates that the SPI time series are multifractal, but its degree differs with aggregation timescale and location.

For pure multifractal series, α decreases with increase in fluctuation, which is quite evident from the results as the SPI-3 series which possesses highest fluctuation among the three cases (3-, 6- and 12-month SPI) considered. Asymmetric index (R) is a useful parameter of multifractal analysis which is computed based on $\Delta\alpha_L$ and $\Delta\alpha_R$, the base width of left- and right-hand branches of the multifractal spectrum, respectively. The different multifractal spectrum parameters can be used as qualitative and quantitative indicators of the dynamics of the meteorological processes (Krzyszczak *et al.*, 2018). Asymmetry index values were obtained for 30 subdivisions and the spatial distribution of values of asymmetry index is presented in Figure 9, which shows that R for most of the subdivisions are positive, SPI-3 series is showing more negative values than SPI-6 and SPI-12, which means that SPI-3 series of subdivisions is showing multifractal spectrum width with right-hand deviation with local low fluctuations. For SPI-12 most of the subdivisions are having positive R value which indicates that left-hand deviation of the multifractal spectrum (right skewed spectra) is likely to have resulted from some degree of local high fluctuations, that is, a fine structure series and extremes are localized. Assam subdivision is having the largest positive R value in SPI-3, SPI-6 and SPI-12. A zero R value indicates that the multifractal spectrum is symmetric (e.g., the R value for SPI 3 series of North Karnataka is practically zero). The negative R value resulting from a spectrum with right-hand deviation (left skewed spectrum) indicates that extreme events play a prominent role in the temporal structure of the time series.

The difference between the maximum and minimum values of $f(\alpha)$ is given by $\Delta f(\alpha)$. The difference $\Delta f(\alpha)$ between maximum and minimum values of the singularity provides an estimate of the spread in changes in fractal patterns. Since $\Delta f(\alpha)$ denotes the frequency ratio of the largest to the smallest fluctuation, $\Delta f(\alpha) > 0$ means that the largest fluctuations are more frequent than smallest fluctuations, while $\Delta f(\alpha) < 0$ denotes the reverse. The spatial distribution of $\Delta f(\alpha)$ is provided in Figure 10. From this figure it is clear that most of the subdivisions are having positive $\Delta f(\alpha)$ values for SPI-3, SPI-6 and SPI-12. This means that largest fluctuations are more frequent than smallest fluctuations.

The spatial variability of α_0 is provided in Figure 11. The values of α_0 range between 0.15 and 0.35, for aggregation timescale 3; 0.25 to 0.5 for the timescale of 6 and 0.4 to 0.75 for an aggregation timescale of 12. This indicates the complexity of SPI-12 series, and an evidence of higher multifractality of SPI-12 series.

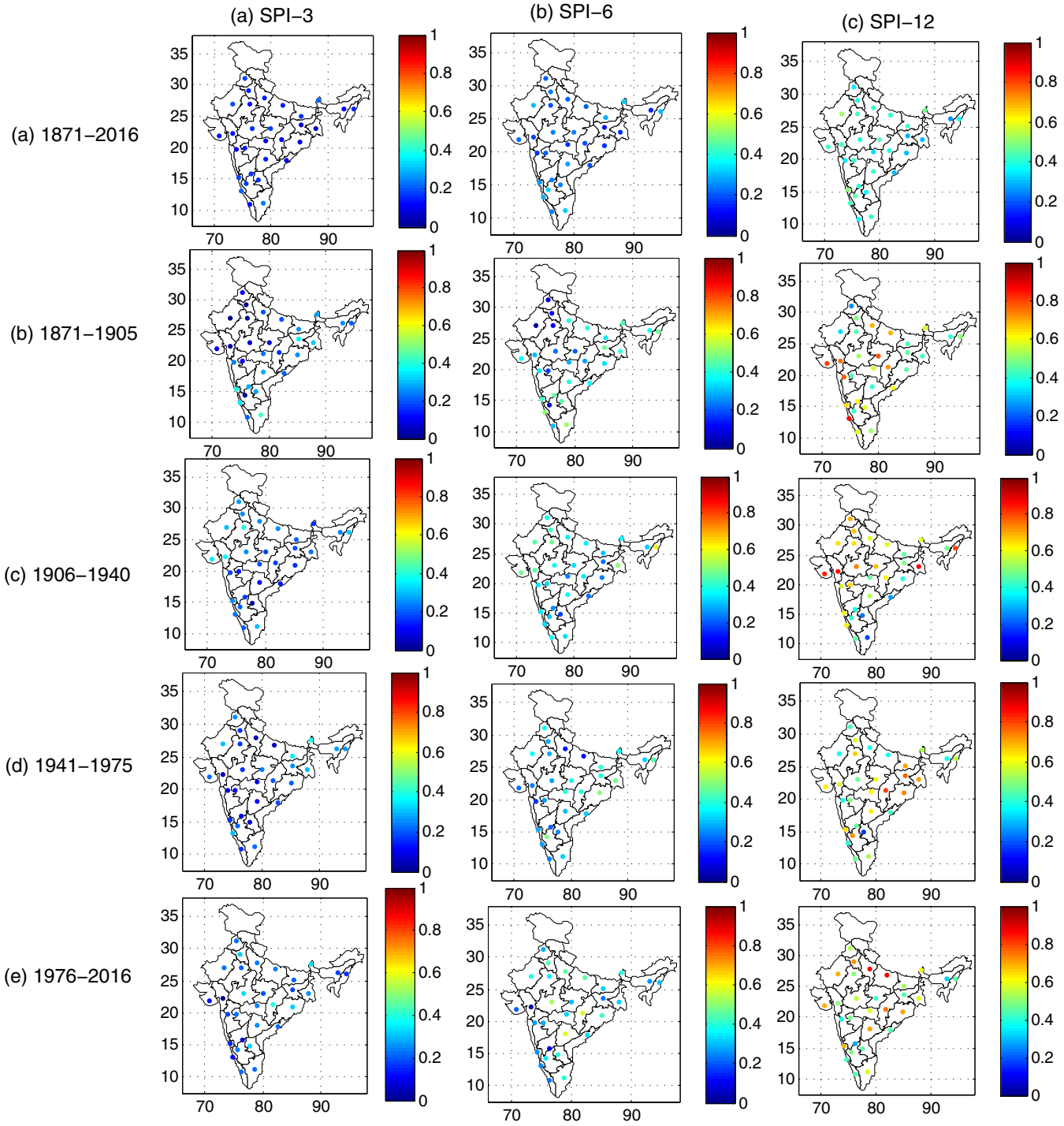

FIGURE 6 Spatial distribution of GHE of SPI 3, 6 and 12 series for different time spells. (a) 1871–2016; (b) 1871–1905; (c) 1906–1940; (d) 1941–1975; (e) 1976–2016 [Colour figure can be viewed at wileyonlinelibrary.com]

In order to explain the variability of the parameters over spatiotemporal scale, the probability density functions (PDF) and CDF are developed using the nonparametric kernel density estimator (Ghosh and Mujumdar, 2007) and the results are presented in Figures 12 and 13, respectively. By examining Figure 12, it is noticed that the parameters the GHE plot is highest for the recent past period (1976–2015) except for SPI-6 series. Also, from Figure 13, it is noticed that there is a right shift of CDF of different parameters for 1976–2016 period, which indicate an increase in these properties in the recent past when compared with the values for different other time spells, except for few cases like spectral width of SPI-6. The Pacific climatic shift of 1976/1977 period is a well debated phenomenon affected the monsoon dynamics of India (Sahana *et al*., 2015). It is logical to hypothesis that it could have an impact on the multifractal characteristics of drought in India. To examine this effect, the drought index series SPI-3, SPI-6 and SPI-12 are partitioned into two as 1871–1976 period and 1977–2016 period. The multiracial characteristics of all the three SPI series are determined for

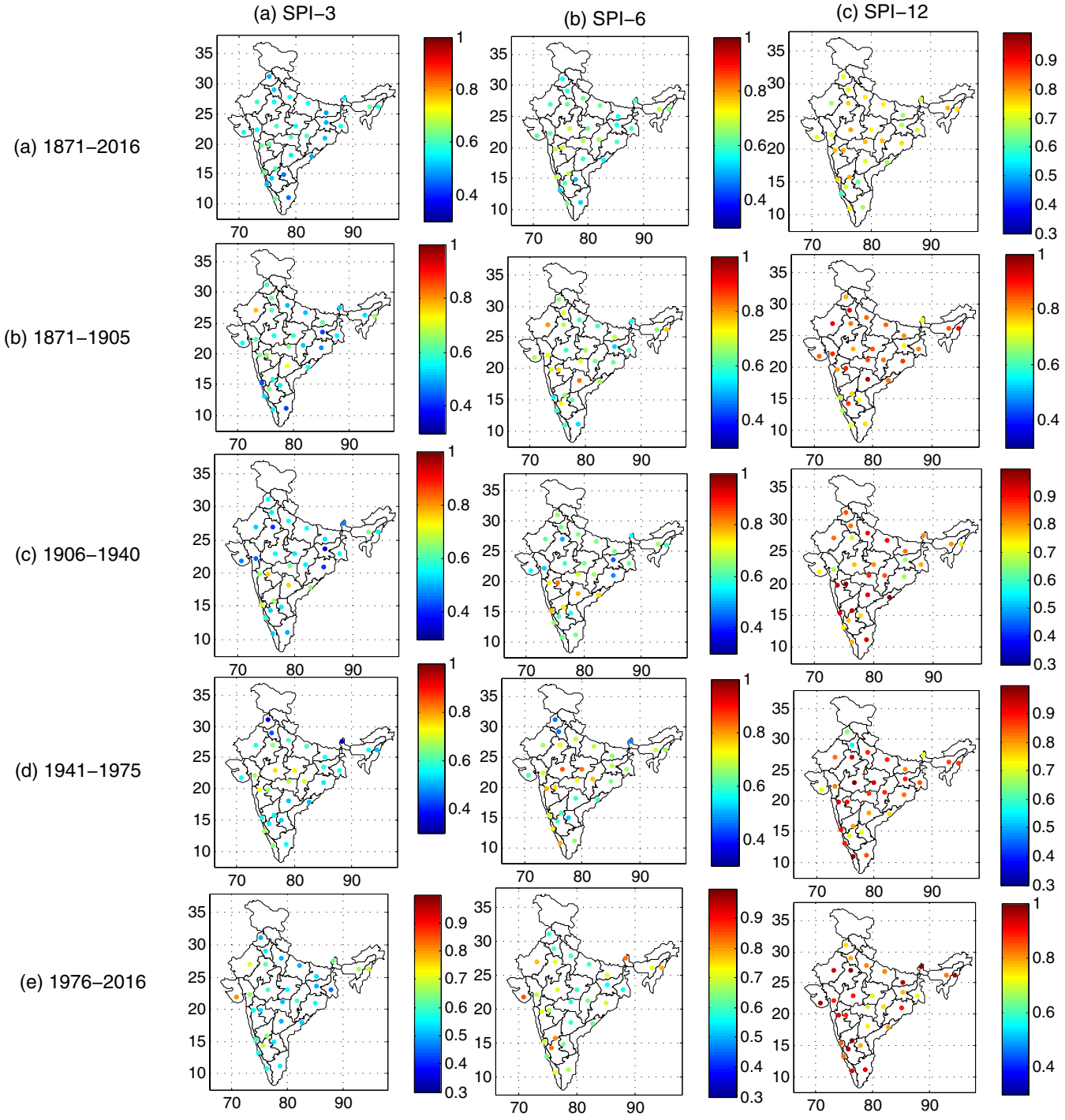

FIGURE 7 Spatial distribution of Hurst exponent (H = $h(2)$) of SPI 3, 6 and 12 series for different time spells. (a) 1871–2016; (b)1871–1905; (c) 1906–1940; (d) 1941–1975; (e) 1976–2016 [Colour figure can be viewed at wileyonlinelibrary.com]

TABLE 3 Properties of multifractal spectra of SPI 3, 6 and 12 time series of four subdivisions

	SPI-3				SPI-6				SPI-12			
Subdivision	$\Delta\alpha_L$	$\Delta\alpha_R$	R	$\Delta\alpha$	$\Delta\alpha_L$	$\Delta\alpha_R$	R	$\Delta\alpha$	$\Delta\alpha_L$	$\Delta\alpha_R$	R	$\Delta\alpha$
WR	−0.137	−0.213	−0.214	0.350	−0.264	−0.276	−0.023	0.540	−0.418	−0.425	−0.008	0.842
SKD	−0.145	−0.106	0.155	0.252	−0.209	−0.181	0.072	0.390	−0.362	−0.316	0.068	0.678
MW	−0.131	−0.125	0.025	0.256	−0.193	−0.152	0.119	0.345	−0.368	−0.295	0.109	0.663
KER	−0.098	−0.130	−0.143	0.228	−0.256	−0.179	0.178	0.435	−0.334	−0.248	0.147	0.582

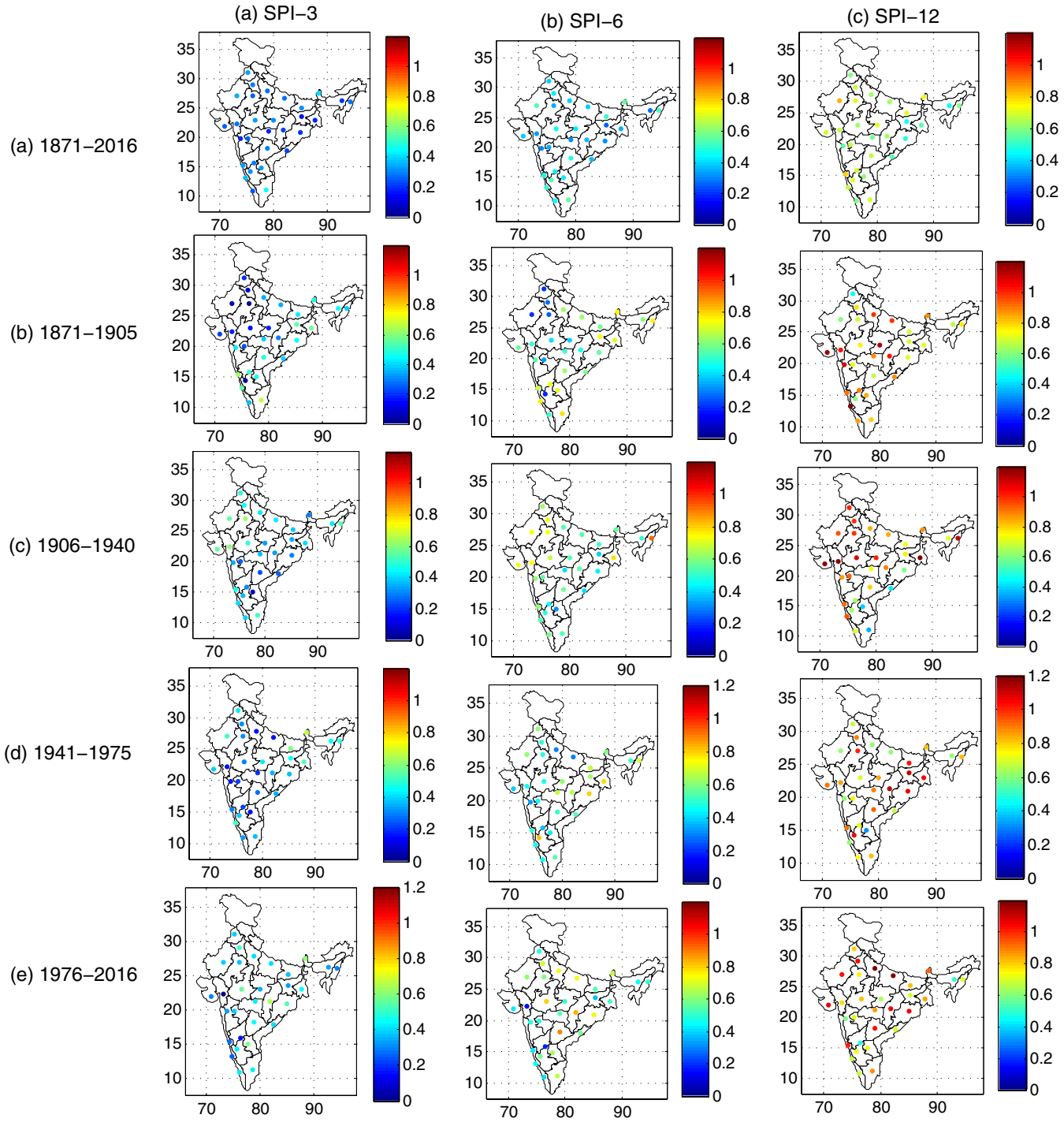

FIGURE 8 Spatial distribution of spectral width of SPI 3, 6 and 12 series for different time spells. (a) 1871–2016; (b) 1871–1905; (c) 1906–1940; (d) 1941–1975; (e) 1976–2016 [Colour figure can be viewed at wileyonlinelibrary.com]

all subdivisions. The CDFs of different parameters for the post- and pre-climatic shift are presented in Figure 14. Figure 14 also depict a clear increase in different multifractal properties in the SPI series of pre and post-1976/1977 period. The results showed that changes in the spectral width and α_0 displayed spatial differences and this imply that the impact on these features is more from local climate processes than the global climate dynamics. The spectral width showed increase for 67% of subdivisions in SPI-3; 70% subdivisions in SPI-6 and 80% subdivisions in SPI-12 series. In the post-1976/77 period, the AI became less positive or even negative in 40, 30 and 47% of the subdivisions in SPI-3, SPI-6 and SPI-12 series, which infer increase or more frequent extreme drought in these subdivisions. The increase in the complexity of drought series could also be attributed to the increased urbanization in the recent past, which is characterized by increased heterogeneity and interaction of various factors such as topography, built environment and the atmosphere (Karatasou and Santamouris, 2018).

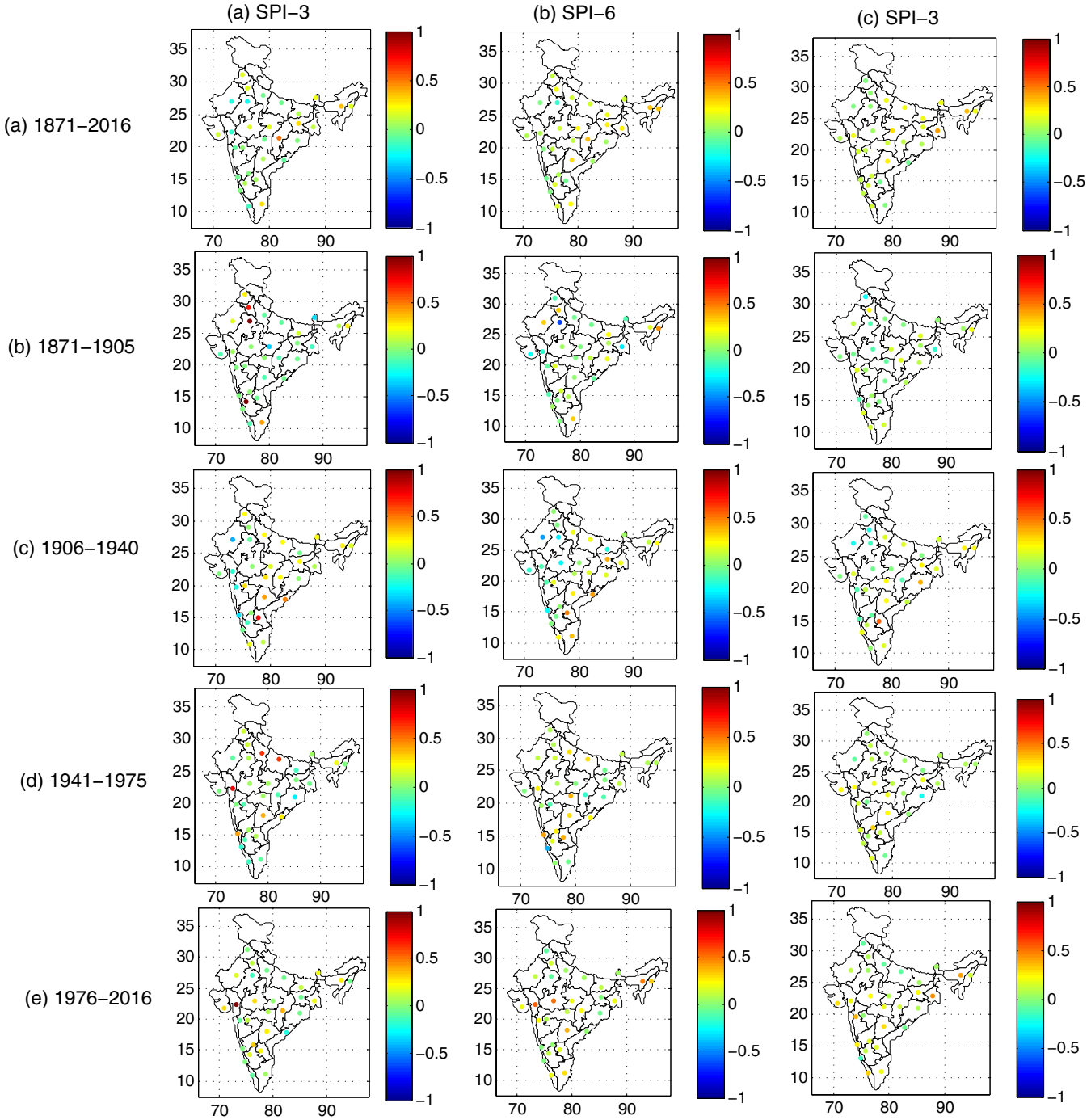

FIGURE 9 Spatial distribution of AI of SPI 3, 6 and 12 series for different time spells. (a) 1871–2016; (b)1871–1905; (c) 1906–1940; (d) 1941–1975; (e) 1976–2016 [Colour figure can be viewed at wileyonlinelibrary.com]

4.3 | Origin of multifractality of drought in India

Determination of the cause of multifractality is one of the common steps in multifractal analysis of hydro-meteorological series. It is popularly known that, the two major causes of multifractality are (Adarsh *et al*., 2019): (a) due to different long-term temporal correlations for small and large fluctuations and (b) due to the broadness (fatness) of PDF, which indicates the variations. In this study, the popular approaches of shuffling and use of surrogate data are adopted to detect the cause of multifractality. The shuffling procedure eliminates any temporal correlations in the data but retaining the distributions as the same. To quantify the influence of the fatness of PDF, the surrogate time series generated from the original can be used. The surrogate series are generated by randomizing their phases in Fourier space, so that the surrogate series are Gaussian. If the multifractality is derived from temporal correlations, the GHE $h(q)$ obtained for the shuffled data is expected to be 0.5. If multifractality is due to broadness of PDF, $h(q)$, obtained for surrogate series, will be independent of q (Movahed *et al*., 2006). If both long-range correlation and

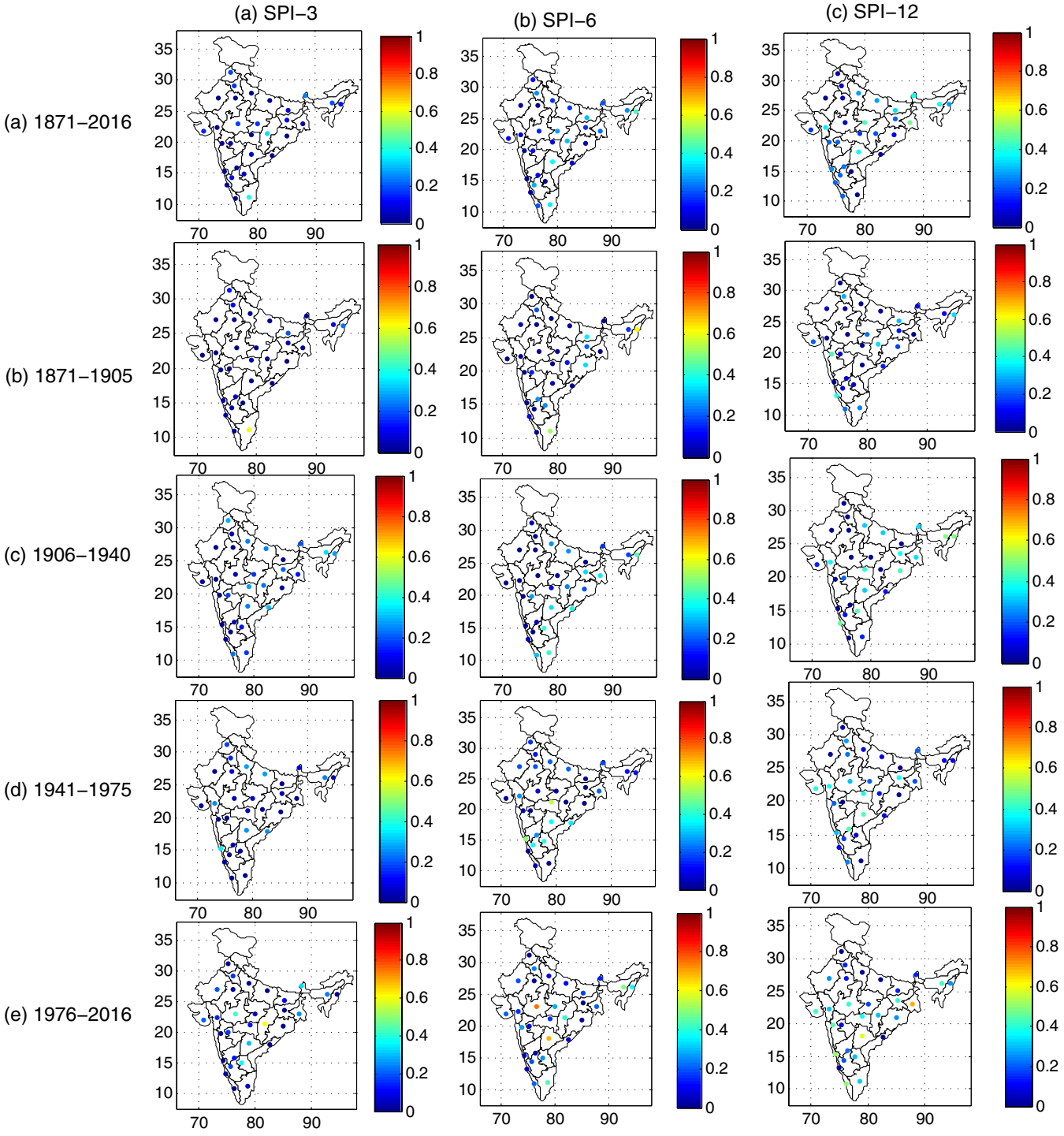

FIGURE 10 Spatial distribution of $\Delta f(\alpha)$ of SPI 3,6 and 12 series for different time spells. (a) 1871–2016; (b) 1871–1905; (c) 1906–1940; (d) 1941–1975; (e) 1976–2016 [Colour figure can be viewed at wileyonlinelibrary.com]

broadness of PDFs are responsible for multifractality, the shuffled and surrogated series will show lower multifractality than the original series. The details of shuffling and the procedure for generating surrogate series through phase randomization can be found elsewhere (Matia *et al*., 2003; Movahed *et al*., 2006; Hou *et al*., 2017). The GHE plots of shuffled surrogated and original estimates of GHE of SPI-12 series are presented in Figure 15 and those for SPI-3 and SPI-12 are presented in Figures S2 and S3, respectively. By examining Figure 12 it is clear that the $h(q)$ values are brought down to zero on shuffling the SPI-12 series of different subdivisions. Therefore, it can be concluded that SPI-12 series is due to the temporal correlations. On examining Figure S1, it is noticed that there is a perfect reduction of $h(q)$ values for SPI-6 series of 20 subdivisions on shuffling, for which multifractality is due to temporal correlations. But on examining Figure S2 it is noticed that in general, there exists a reduction in $h(q)$ value on shuffling,

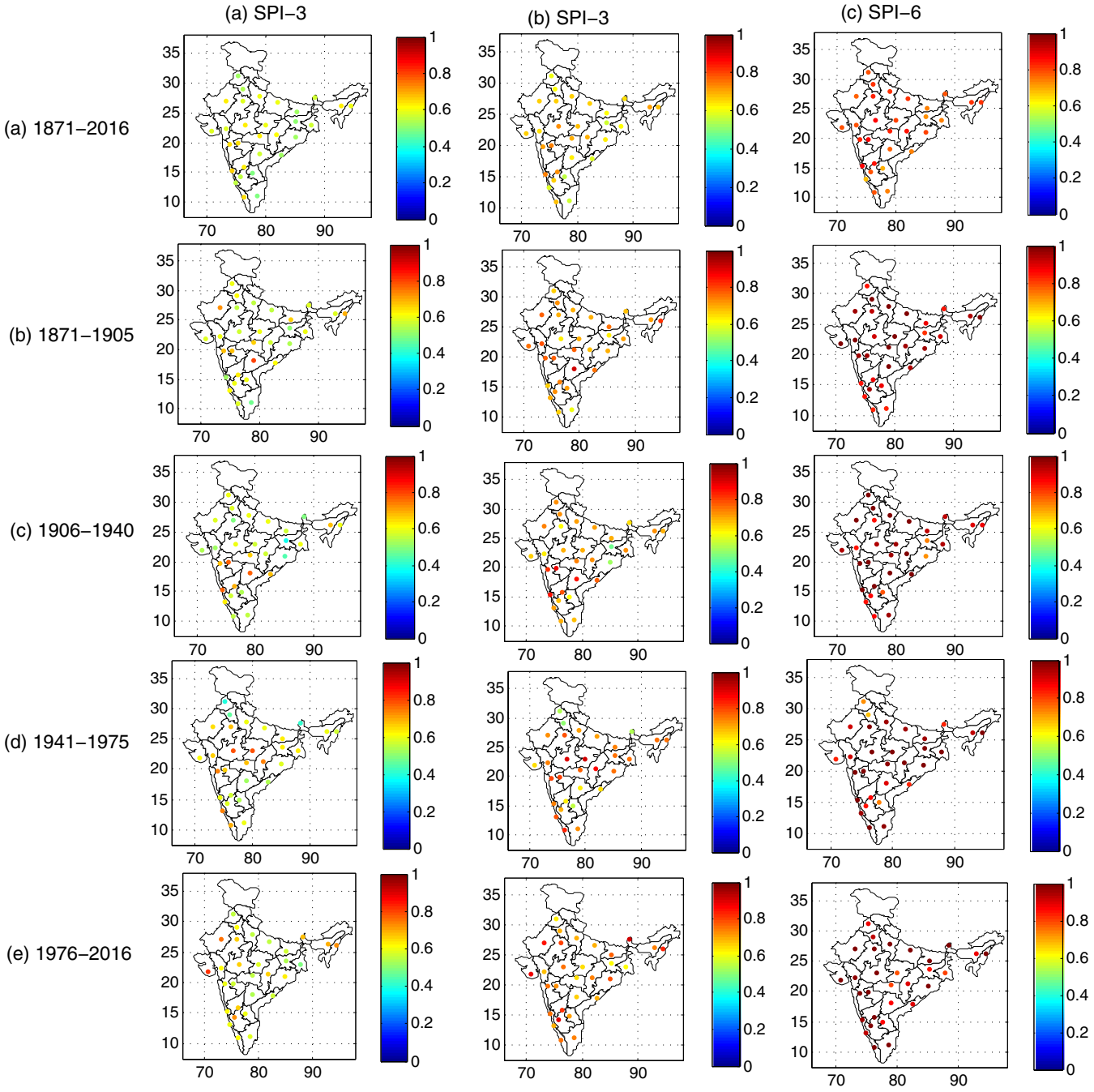

FIGURE 11 Spatial distribution of α_0 of SPI 3, 6 and 12 series for different time spells. (a) 1871–2016; (b) 1871–1905; (c) 1906–1940; (d) 1941–1975; (e) 1976–2016 [Colour figure can be viewed at wileyonlinelibrary.com]

but the correlations are not destroyed in full. Thus, it can be ascertained that the multifractality of SPI-12 series is due to both correlation and broadness of PDF.

4.4 | Discussion

This study performed the multifractal characterization of drought index of 30 meteorological subdivisions in India computed at three different aggregation timescales. Also, it has investigated the causes of multifractality and variability of multifractal properties in the different time spells of the last century. The multifractal properties of precipitation-based drought index like SPI could be linked with the physical mechanisms leading to the precipitation of the study area (Hou *et al.*, 2017). The precipitation in the Indian subcontinent is influenced by different physical processes, oceanic and atmospheric circulations, topography and local processes. The variability of drought is influenced by annual, intra-seasonal to seasonal, inter-annual and inter-decadal timescales. The oceanic proximity plays a dominant role in the precipitation of the country as the country is bounded by Arabian Sea, Indian Ocean and Bay of Bengal in the west, south and eastern parts of the country. However, it will be hard to find a universal pattern such as

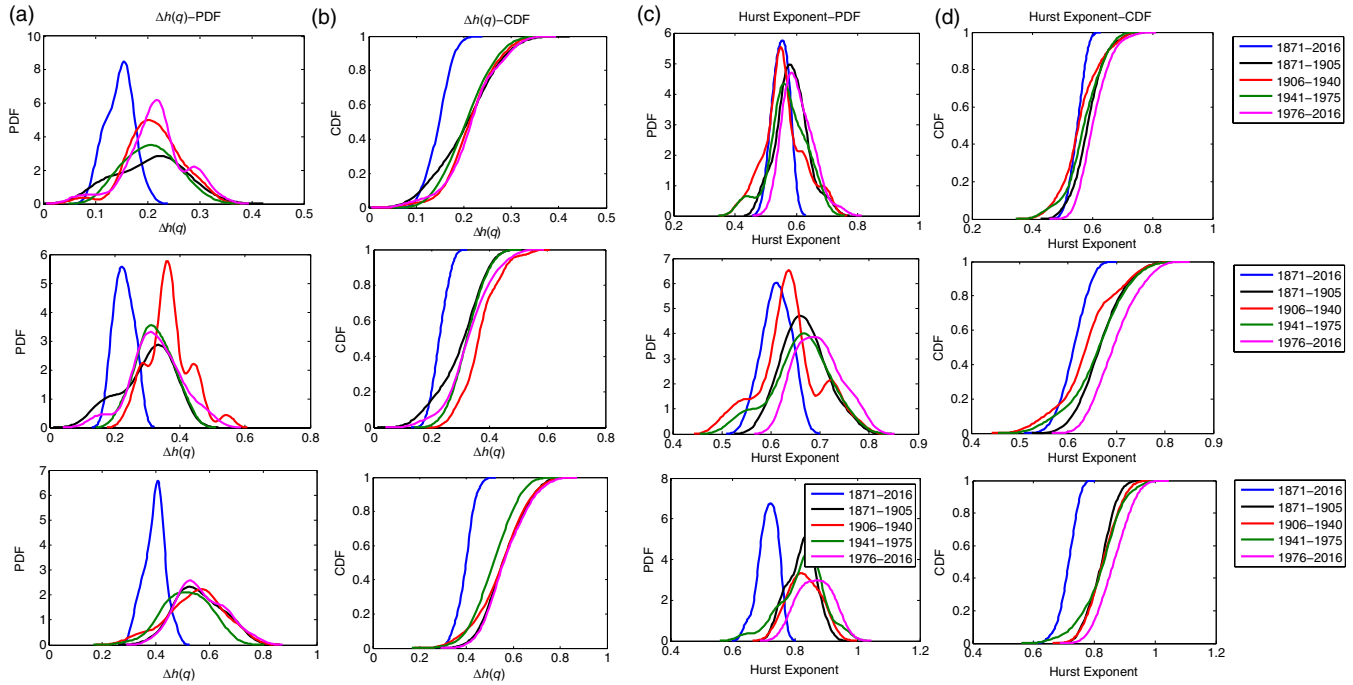

FIGURE 12 Spatiotemporal variability of parameters of GHE plot (a, b) are the PDF and CDF plots of $\Delta h(q)$ over different time spells. (c, d) are the PDF and CDF plots of Hurst exponent ($h(2)$) over different time spells. Upper panels show the results of SPI-3 series; middle panels show the results of SPI-6 series and lower panels show the results of SPI-12 series [Colour figure can be viewed at wileyonlinelibrary.com]

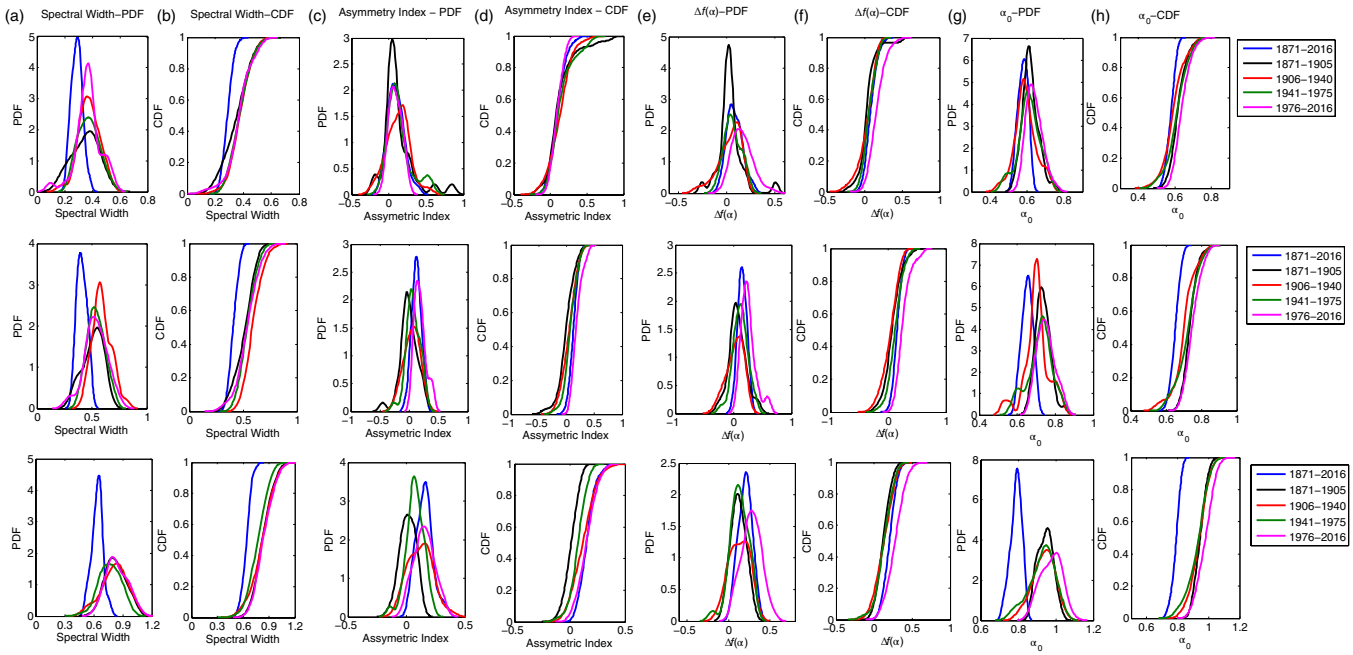

FIGURE 13 Spatiotemporal variability of parameters of multifractal spectrum: (a, b) are the PDF and CDF plots of spectral width; (c, d) are the PDF and CDF plots of asymmetry index; (e, f) are the PDF and CDF plots of $\Delta f(\alpha)$; (g, h) are the PDF and CDF plots of α_0, over different time spells. Upper panels show the results of SPI-3 series; middle panels show the results of SPI-6 series and lower panels show the results of SPI-12 series [Colour figure can be viewed at wileyonlinelibrary.com]

how the exponents change with latitude, altitude or distance from the coast (Orun and Kocak, 2009). Also attributing the reason for multifractal to single indicator is quite impossible as the Indian monsoon system is quite complex (Wang *et al.*, 2015) and many local processes and details like moisture, terrain, vegetation affect may influence the regional precipitation variations (Yuan *et al.*, 2010). It was well proven that the large-scale atmospheric circulations such as Quasi-Biennial Oscillation (QBO), El Niño–Southern Oscillations (ENSO), Equatorial Indian Ocean Oscillation (EQUINOO), North Atlantic Oscillation (NAO), Atlantic Multidecadal Oscillation, etc. are all

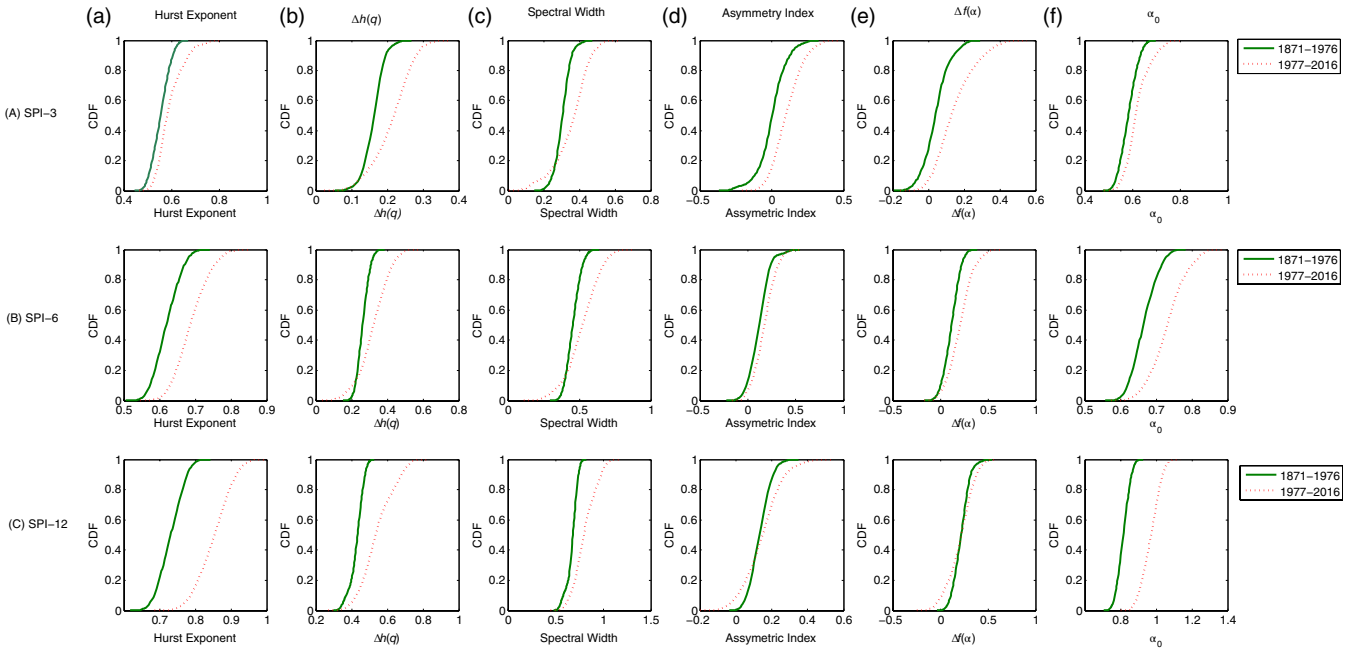

FIGURE 14 Temporal variability of GHE plot parameters and parameters of multifractal spectrum: (a) Hurst exponent; (b) $\Delta h(q)$; (c) spectral width; (d) asymmetry index; (e) $\Delta f(\alpha)$; (f) α_0. Upper panels show the results of SPI-3 series; middle panels show the results of SPI-6 series and lower panels show the results of SPI-12 series [Colour figure can be viewed at wileyonlinelibrary.com]

playing a major role on southwest monsoon rainfall of the summer season in India (Gadgil *et al*., 2004; Goswami *et al*., 2006; Maity and Nagesh Kumar, 2006; 2007). Thus, meteorological droughts of different aggregation timescales could be linked with such climatic oscillations (Joshi *et al*., 2016; Rashid *et al*., 2018). The authors' investigations found that the dominant period of short-term drought index is 2–3 years (typical of QBO); the dominant period of SPI-

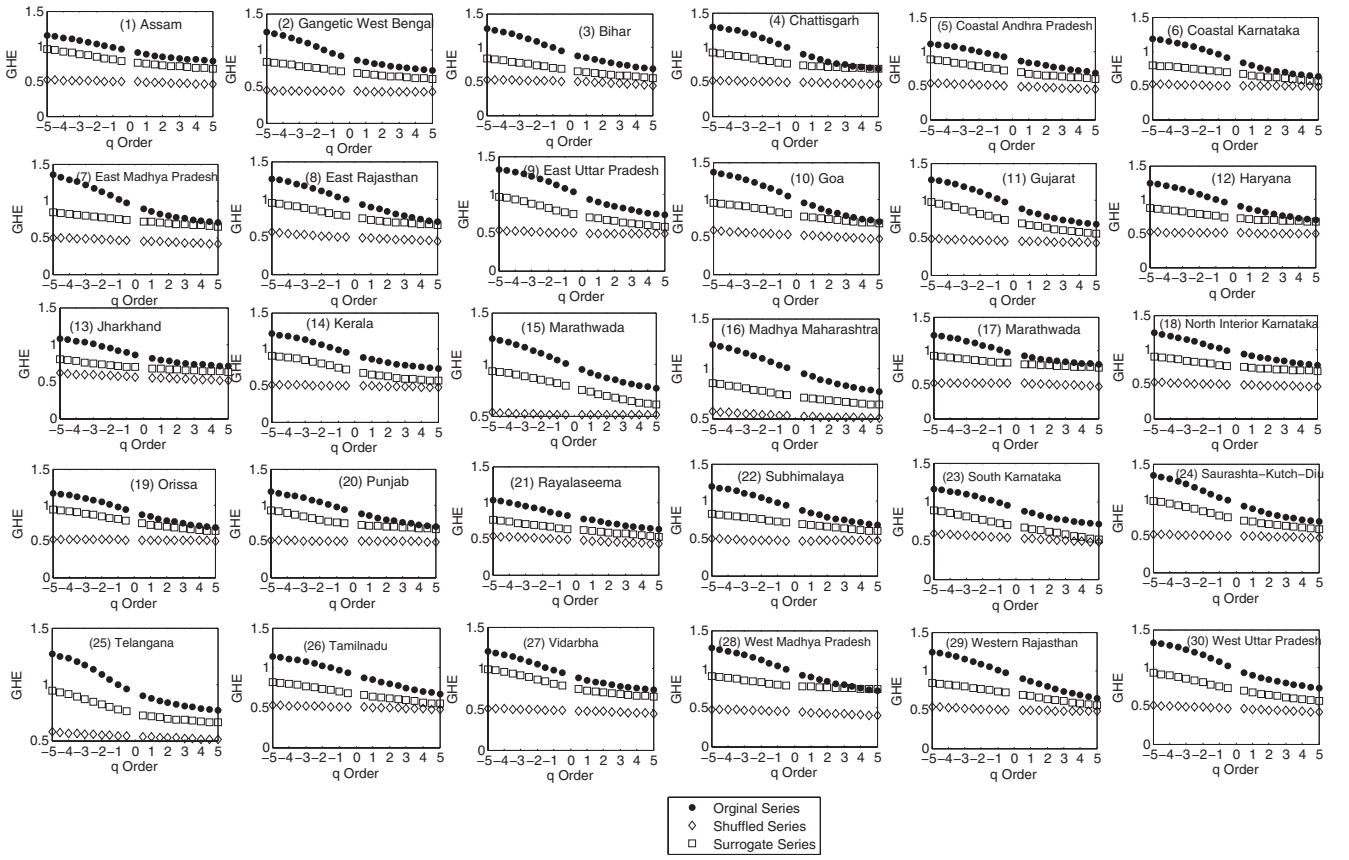

FIGURE 15 GHE plots of original, shuffled and surrogate series of SPI-12 of different subdivisions

6 is found to be 5–8 years (typical periodicity of ENSO) and SPI-12 is found to be 50–60 years (periodicity of Atlantic Oscillations) with distinct spatial variability. Apart from the influence of the large-scale circulations, the increased convective activity over the western part of Indian Ocean may also influence the precipitation in major basins of northern India. Despite this, our study finds that the climatic differences (low rainfall being received in WR subdivision to high rainfall in regions like Kerala) are not found to have any dominant influence on the multifractal properties of drought, which may be because the original structure of the daily precipitation series might have been distorted by the aggregation operation in the estimation of drought indices. Ascertaining the role of persistence is vital to the development of hydrological models and the changes in the hydrological persistence over the time spell are to be investigated (Dey and Mujumdar, 2018). These may influence the inter-arrival times of extreme and rare events and also help in assessing the underlying mechanisms of their return periods (Koscielny-Bunde *et al*., 2003). Also, the changes in the persistence properties need to be ascertained, as such information can contribute much in choosing the right model for the application of prediction of the hydrological variables. Any significant change in the persistence may lead to erroneous predictions and the situation is quite analogous to the use of a stationarity assumption under a non-stationary environment in a changing climate scenario.

Even though multifractality of hydro-meteorological time series is well debated in literature, the subsequent extension of the use of these parameters for practical hydrological simulation or prediction is limited. But certain studies give an insight on the link between trend of the series and multifractality; while the value of H (an indicative of short/-long memory of the time series) can be linked with the autocorrelation structure of the series (Bassingthwaighte and Beyer, 1991; Bassingthwaighte and Raymond, 1995), even though such relations are valid/works well for high value of say $H > 0.7$. The scaling information derived from the multifractal analysis can be used for multifractal modelling, simulation and synthetic generation of rainfall fields (Deidda, 1999; 2000; Deidda *et al*., 1999; Serinaldi, 2010). Multifractal models with different frame works could be developed for simulation or prediction of hydrological variables based on the parameters obtained (Tessier *et al*., 1996; Kantelhardt *et al*., 2003; Kantelhardt *et al*., 2006), which is a very promising domain for subsequent research. The scaling exponents can be used for derivation of intensity–duration–frequency curves for rainfall disaggregation (Veneziano and Furcolo, 2002; Huang *et al*., 2014). The space–time disaggregation of rainfall is a possible application for the scaling exponents developed (Deidda, 2000; Hubert, 2001; Pathirana *et al*., 2007). Prediction in ungauged basins is another challenging but potential research domain and the scaling exponents derived can be useful for such studies (Schertzer *et al*., 2007).

This paper investigated the multifractal properties of a popular drought index (SPI) of different meteorological subdivisions of India. The knowledge of long/short memory persistence of SPI gives new insights in the prediction selection of time series modelling of droughts in India using classical or data driven approaches. The evidence of multifractality in time series of drought may also be helpful to develop the multifractal models and subsequent risk assessments of droughts. All these parameters are particular characteristics of the data analysed and the scale at which they are analysed. From the results it can be observed that there is significant variation in these values over different regions and over different aggregation timescales.

5 | CONCLUSIONS

In this research work we investigated the fractal properties of SPI time series (at 3-, 6- and 12-month aggregation scales indicating short, medium- and long-term droughts) of 30 meteorological subdivisions in India using MF-DFA method to verify the non-linearity and complexity of the drought dynamics. The major conclusions of the study are:

- The q-dependence of the GHE ($h(q)$plots) and plot of fluctuation function with scale and the shape of multifractal spectrum indicated that the SPI values of all the subdivisions show multifractal behaviour.
- Hurst exponent and degree of multifractality of SPI series of all subdivisions increase with increase in aggregation timescale.
- SPI-3 of Tamil Nadu, Coastal Andhra Pradesh, Rayalaseema, Bihar, Punjab, Jharkhand show short-term persistency while SPI-6 and SPI-12 of all subdivisions show long-term persistency.
- The multifractal properties of drought show an increase in the post-1976 period, which could be attributed to the effect of urbanization and climatic shift of 1976/1977 period, which introduced more heterogeneity to precipitation series.
- The multifractality of SPI-12 series in India is due to correlation properties but those of SPI-3 series is due to both correlation properties and broadness of PDF.

CONFLICT OF INTEREST

The authors declare no potential conflict of interests.

ORCID

S. Adarsh https://orcid.org/0000-0001-8223-043X

REFERENCES

Adarsh, S., Dharan, D.S., Anuja, P.K. and Suman, A. (2019) Unravelling the scaling characteristics of daily streamflows of Brahmani River basin, India using arbitrary order Hilbert spectral and detrended fluctuation analyses. *SN Applied Sciences*, 1, 58. https://doi.org/10.1007/s42452-018-0056-1.

Adarsh, S. and Janga Reddy, M. (2015) Trend analysis of rainfall in four meteorological subdivisions of southern India using nonparametric methods and discrete wavelet transforms. *International Journal of Climatology*, 35(6), 1107–1124.

Adarsh, S., Karthik, S., Shyma, M., Das, P.G., Shirin Parveen, A.T. and Narayan, S. (2018) Developing short term drought severity–duration–frequency curves for Kerala meteorological subdivision, India using bivariate copulas. *KSCE Journal of Civil Engineering*, 22(3), 962–973.

Baranowski, P., Krzyszczak, J., Slawinski, C., Hoffmann, H., Kozyra, J., Nieróbca, A., Siwek, K. and Gluza, A. (2015) Multifractal analysis of meteorological time series to assess climate impacts. *Climate Research*, 65, 39–52.

Bassingthwaighte, J.B. and Beyer, R.P. (1991) Fractal correlation in heterogeneous systems. *Physica D*, 53, 71–84.

Bassingthwaighte, J.B. and Raymond, G.M. (1995) Evaluation of the dispersional analysis method for fractal time series. *Annals of Biomedical Engineering*, 23(4), 491–505.

Bazrafshan, J., Hejabi, S. and Rahimi, J. (2013) Drought monitoring using the multivariate standardized precipitation index (MSPI). *Water Resource Management*, 28(4), 1045–1060.

Burgueño, A., Lana, X., Serra, C. and Martínez, M.D. (2014) Daily extreme temperature multifractals in Catalonia (NESpain). *Physics Letters A*, 378(2014), 874–885.

Dahlstedt, K. and Jensen, H. (2005) Fluctuation spectrum and size scaling of river flow and level. *Physica A: Statistical Mechanics and its Applications*, 348, 596–610.

Deidda, R. (1999) Multifractal analysis and simulation of rainfall fields in space. *Physics and Chemistry of the Earth, Part B: Hydrology, Oceans and Atmosphere*, 24(1–2), 73–78.

Deidda, R. (2000) Rainfall downscaling in a space-time multifractal framework. *Water Resources Research*, 36(7), 1779–1794.

Deidda, R., Benzi, R. and Siccardi, F. (1999) Multifractal modeling of anomalous scaling laws in rainfall. *Water Resources Research*, 35(6), 1853–1867.

Dey, P. and Mujumdar, P.P. (2018) Multiscale evolution of persistence of rainfall and streamflow. *Advances in Water Resources*, 121, 285–303.

Gadgil, S., Vinayachandran, P.N., Francis, P.A. and Gadgil, S. (2004) Extremes of the Indian summer monsoon rainfall, ENSO and equatorial Indian Ocean Oscillation. *Geophysical Research Letters*, 31, L12213. https://doi.org/10.1029/2004GL019733.

Ganguli, P. and Janga Reddy, M. (2013) Evaluation of trends and multivariate frequency analysis of droughts in three meteorological subdivisions of western India. *International Journal of Climatology*, 34(3), 911–928.

Ghosh, S. and Mujumdar, P.P. (2007) Non-parametric methods for modeling GCM and scenario uncertainty in drought assessment. *Water Resources Research*, 43(7), W07405. https://doi.org/10.1029/2006WR005351.

Goswami, B.N., Madhusoodanan, M.S., Neema, C.P. and Sengupta, D. (2006) A physical mechanism for North Atlantic SST influence on the Indian summer monsoon. *Geophysical Research Letters*, 33, L02706. https://doi.org/10.1029/2005GL024803.

Guhathakurta, P. and Rajeevan, M. (2008) Trends in the rainfall pattern over India. *International Journal of Climatology*, 28(11), 1453–1469.

Guhathakurta, P., Rajeevan, M., Sikka, D.R. and Tyagi, A. (2015) Observed changes in southwest monsoon rainfall over India during 1901–2011. *International Journal of Climatology*, 35, 1881–1898.

Hajian, S. and Movahed, M.S. (2010) Multifractal detrended cross-correlation analysis of sunspot numbers and river flow fluctuations. *Physica A: Statistical Mechanics and its Applications*, 389(21), 4942–4957.

Hou, W., Feng, G., Yan, P. and Li, S. (2017) Multifractal analysis of the drought area in seven large regions of China from 1961 to 2012. *Meteorology and Atmospheric Physics*, 130(4), 459–471.

Hou, W., Peng-Cheng, Y., Shu-Ping, L., Gang, T. and Jing-Guo, H. (2015) Application of long-range correlation and multi-fractal analysis for the depiction of drought risk. *Chinese Physics B*, 25(1), 019201.

Huang, Q., Chen, Y., Xu, S. and Liu, J. (2014) Case study of applying multifractal models for rainfall IDF analysis in China. *Journal of Hydrologic Engineering*, 19(1), 205–210. https://doi.org/10.1061/(ASCE)HE.1943-5584.0000781.

Hubert, P. (2001) Multifractals as a tool to overcome scale problems in hydrology. *Hydrological Sciences Journal*, 46(6), 897–905.

Hurst, H.E. (1951) Long-term storage capacity of reservoirs. *Transactions of the American Society of Civil Engineers*, 116, 770–808.

Hurst, H.E., Black, R.P. and Simaika, Y.M. (1965) *Long-Term Storage: An Experimental Study*. London: Constable.

Ihlen, E.A.F. (2012) Introduction to multifractal detrended fluctuation analysis in MATLAB. *Frontiers in Physiology*, 3, 141. https://doi.org/10.3389/fphys.2012.00141.

Joshi, N., Gupta, D., Suryavanshi, S., Adamowski, J. and Madramootoo, C.A. (2016) Analysis of trends and dominant periodicities in drought variables in India: a wavelet transform based approach. *Atmospheric Research*, 182, 200–220.

Kantelhardt, J.W., Bunde, E.K., Rybski, D., Barun, P., Bunde, A. and Havlin, S. (2006) Long-term persistence and multifractality of precipitation and river runoff records. *Journal of Geophysical Research: Atmospheres*, 28, 1–13.

Kantelhardt, J.W., Rybski, D., Zschiegner, S.A., Braun, P., Koscielny-Bunde, E., Livina, V., Havlin, S. and Bunde, A. (2003) Multifractality of river runoff and precipitation: comparison of fluctuation analysis and wavelet methods. *Physica A*, 330, 240–245.

Kantelhardt, J.W., Zschiegner, S.A., Koscielny-Bunde, E., Halvin, H., Bunde, A. and Stanley, H.E. (2002) Multifractal detrended fluctuation analysis of nonstationary time series. *Physica A: Statistical Mechanics and its Applications*, 316, 87–114.

Karatasou, S. and Santamouris, M. (2018) Multifractal analysis of high-frequency temperature time series in the urban environment. *Climate*, 6, 50. https://doi.org/10.3390/cli6020050.

Koscielny-Bunde, E., Kantelhardt, J.W., Braun, P., Bunde, A. and Havlin, S. (2003) Long-term persistence and multifractality of river runoff records: detrended fluctuation studies. *Journal of Hydrology*, 322, 120–137.

Kothawale, D.R. and Rajeevan, M. (2017) *Monthly, seasonal and annual rainfall time series for All-India, homogeneous regions and meteorological subdivisions: 1871–2016*. Pune: Indian Institute of Tropical Meteorology (IITM). Research report number: RR-138.

Krishnakumar, K.N., Rao, G.S.L.H.V.P. and Gopakumar, C.S. (2009) Rainfall trends in twentieth century over Kerala, India. *Atmospheric Environment*, 43, 1940–1194.

Krzyszczak, J., Baranowski, P., Zubik, M., Kazandjiev, V., Georgieva, V., Sławiński, C., Siwek, K., Kozyra, J. and Nieróbca, A. (2018) Multifractal characterization and comparison of meteorological time series from two climatic zones. *Theoretical and Applied Climatology*, 1–14. https://doi.org/10.1007/s00704-018-2705-0.

Li, E., Mu, X., Zhao, G. and Gao, P. (2015) Multifractal detrended fluctuation analysis of streamflow in Yellow River basin, China. *Water*, 7, 1670–1686.

McKee, T.B., Doesken, N.J. and Kleist, J. (1993) The relationship of drought frequency and duration to time scales. In: *8th Conference on Applied Climatology*, Vol. 17–22. Anaheim, California, pp. 179–184.

Maity, R. and Nagesh Kumar, D. (2006) Hydroclimatic association of monthly summer monsoon rainfall over India with large-scale atmospheric circulation from tropical Pacific Ocean and Indian Ocean region. *Atmospheric Science Letters*, 7(4), 101–107.

Maity, R. and Nagesh Kumar, D. (2007) Hydroclimatic teleconnection between global sea surface temperature and rainfall over India at subdivisional monthly scale. *Hydrologic Processes*, 21(14), 1802–1813.

Mandelbrot, B. (1974) Intermittent turbulence in self-similar cascades: divergence of high moments and dimension of the carrier. *Journal of Fluid Mechanics*, 62, 331–358.

Mandelbrot, B. (1982) *The Fractal Geometry of Nature*. New York, NY: WH Freeman.

Matia, K., Ashkenazy, Y. and Stanley, H.E. (2003) Multifractal properties of price fluctuations of stocks and commodities. *Europhysics Letters*, 61, 422–428.

Movahed, M.S., Jafari, G.R., Ghasemi, F., Rahvar, S. and Tabar, M.R.R. (2006) Multifractal detrended fluctuation analysis of sunspot time series. *Journal of Statistical Mechanics*, 2, P02003.

Olsson, J. and Niemczynowicz, J. (1996) Multifractal analysis of daily spatial rainfall distributions. *Journal of Hydrology*, 187(1–2), 29–43.

Orun, M. and Kocak, K. (2009) Applicatıon of detrended fluctuation analysis to temperature data from Turkey. *International Journal of Climatology*, 29(14), 2130–2136.

Pai, D.S., Sridhar, L., Guhathakurta, P. and Hatwar, H.R. (2011) District wise drought climatology of the southwest monsoon season over India based on standardized precipitation index. *Natural Hazards*, 59, 1797–1813.

Palmer, W.C. (1965) *Meteorological drought*. Washington, DC: U.S. Weather Bureau. Research paper 45, p. 58.

Pandey, G., Lovejoy, S. and Schertzer, D. (1998) Multifractal analysis of daily river flows including extremes for basins five to two million square kilometers, one day to 75 years. *Journal of Hydrology*, 208, 62–81.

Parthasarathy, B., Munot, A.A. and Kothawale, D.R. (1995) *Monthly and seasonal rainfall series for all-India, Homogeneous Regions and Meteorological subdivisions: 1871–1994*. Pune: Indian Institute of Tropical Meteorology (IITM). Research report number: RR-065, IIIN 0252-1075.

Pathirana, P., Herath, S. and Yamada, T. (2007) Estimating rainfall distributions at high temporal resolutions using a multifractal model. *Hydrology and Earth System Sciences Discussion*, 7(5), 668–679.

Peng, C.K., Buldyrev, S.V., Simons, M., Stanley, H.E. and Goldberger, A.L. (1994) Mosaic organization of DNA nucleotides. *Physical Review E*, 49, 1685–1689.

Rashid, M.M., Johnson, F. and Sharma, A. (2018) Identifying sustained drought anomalies in hydrological records: a wavelet approach. *Journal of Geophysical Research: Atmospheres*, 123(14), 7416–7432.

Rego, C.R.C., Frota, H.O. and Gusmão, M.S. (2013) Multifractality of Brazilian rivers. *Journal of Hydrology*, 495, 208–215.

Sahana, A.S., Ghosh, S., Ganguly, A. and Murtugudde, R. (2015) Shift in Indian summer monsoon onset during 1976/1977. *Environmental Research Letters*, 10, 054006.

Schertzer, D., Hubert, P. and Lovejoy, S. (2007) Scaling, multifractals and predictions in ungauged basins: where we have been, where we are going? In: *Predictions in Ungauged Basins: PUB Kick-off (Proceedings of the PUB Kick-Off Meeting Held in Brasilia, 20–22 November 2002)*, Vol. 309. Wallingford: IAHS Publications, pp. 92–101.

Serinaldi, F. (2010) Multifractality, imperfect scaling and hydrological properties of rainfall time series simulated by continuous universal multifractal and discrete random cascade models. *Nonlinear Processes in Geophysics*, 17(6), 697–714.

Tan, X. and Gan, T.W. (2017) Multifractality of Canadian precipitation and streamflow. *International Journal of Climatology*, 37(S1), 1221–1236.

Tatli, H. (2015) Detecting persistence of meteorological drought *via* the Hurst exponent. *Meteorological Applications*, 22, 763–769.

Tessier, Y., Lovejoy, S., Hubert, P., Schertzer, D. and Pecknold, S. (1996) Multifractal analysis and modeling of rainfall and river flows and scaling, causal transfer functions. *Journal of Geophysical Research: Atmospheres*, 101, 26427–26440.

Thomas, J. and Prasannakumar, V. (2016) Temporal analysis of rainfall (1871–2012) and drought characteristics over a tropical monsoon-dominated state (Kerala) of India. *Journal of Hydrology*, 534, 266–280.

Thomas, T., Nayak, P.C. and Ghosh, N.C. (2015) Spatio-temporal analysis of drought characteristics in the Bundelkhand region of central India using the standardized precipitation index. *Journal of Hydrological Engineering*, 20 (11), 05015004. https://doi.org/10.1061/(ASCE)HE.1943-5584.0001189.

Van-Rooy, M.P. (1965) A rainfall anomaly index (RAI) independent of time and space. *Notos*, 14, 43–48.

Veneziano, A. and Furcolo, P. (2002) Multifractality of rainfall and scaling of intensity-duration-frequency curves. *Water Resources Research*, 38, 12): 1–12):12.

Vicente-Serrano, S.M., Begueria, S., Lopez-Moreno, J.I., Angulo, M. and El Kenawy, A. (2010) A new global 0.5 degrees gridded dataset (1901–2006) of a multiscalar drought index: comparison with current drought index datasets based on the Palmer drought severity index. *Journal of Hydrometeorology*, 11, 1033–1043.

Wang, B., Xiang, B., Li, J., Webster, P.J., Rajeevan, M.N., Liu, J. and Ha, K.-J. (2015) Rethinking Indian monsoon rainfall prediction in the context of recent global warming. *Nature Communications*, 6, 7154. https://doi.org/10.1038/ncomms8154.

Yu, Z.G., Leung, Y., Chen, Y.D., Zhang, Q., Anh, V. and Zhou, Y. (2014) Multifractal analyses of daily rainfall time series in Pearl River basin of China. *Physica A: Statistical Mechanics and its Applications*, 405, 193–202.

Yuan, N., Fu, Z. and Mao, J. (2010) Different scaling behaviors in daily temperature records over China. *Physica A: Statistical Mechanics and its Applications*, 389(19), 4087–4095.

Zargar, A., Sadiq, R., Naser, B. and Khan, F.I. (2011) A review of drought indices. *Environmental Reviews*, 19, 333–349.

Zhang, Q., Chong, Y.X., Yu, Z.G., Liu, C.L. and David Chen, Y.Q. (2009a) Multifractal analysis of streamflow records of the East River basin (Pearl River), China. *Physica A: Statistical Mechanics and its Applications*, 388, 927–934.

Zhang, Q., Lu, W., Chen, S. and Liang, X. (2016) Using multifractal and wavelet analyses to determine drought characteristics: a case study of Jilin province, China. *Theoretical and Applied Climatology*, 125, 829–840.

Zhang, Q., Xu, C.Y., David Chen, Y.Q., Gemmer, M. and Yu, Z.G. (2008) Multifractal detrended fluctuation analysis of streamflow series of the Yangtze River basin, China. *Hydrological Processes*, 22, 4997–5003.

Zhang, Q., Yu, Z., Xu, C. and Anh, V. (2009b) Multifractal analysis of measure representation of flood/drought grade series in the Yangtze delta, China, during the past millennium and their fractal model simulation. *International Journal of Climatology*, 30, 450–457.

SUPPORTING INFORMATION

Additional supporting information may be found online in the Supporting Information section at the end of this article.

How to cite this article: Adarsh S, Kumar DN, Deepthi B, Gayathri G, Aswathy SS, Bhagyasree S. Multifractal characterization of meteorological drought in India using detrended fluctuation analysis. *Int J Climatol*. 2019;1–22. https://doi.org/10.1002/joc.6070

APPENDIX: DESCRIPTION OF MULTIFRACTAL PARAMETERS

The slope of log-linear fit of the plot between fluctuation function ($F_s(q)$) and scale (s) for different moment orders (q) gives the GHE ($h(q)$). The Hurst exponent ($H = h(2)$) is only one of the several types of scaling exponents used to parameterize the multifractal structure of the time series. The q-order mass exponent ($\tau(q)$) and singularity exponent (α) are alternative measures to comment on the multifractality of time series. The Hurst exponent ($h(2)$) helps to comment on long/short memory persistence, while other two exponents are helpful in providing information on degree of multifractality and singularity of the time series. These exponents can be mathematically estimated as

$$\tau(q) = qh(q) - 1, \tag{A1}$$

$$\alpha = \frac{d\tau(q)}{dq}, \tag{A2}$$

$$f(\alpha) = q\alpha - \tau(q), \tag{A3}$$

where $f(\alpha)$ provides the singularity spectrum. The dependency of $h(q)$ on q indicates the multifractal nature of the time series and the difference in the slopes of the segments before and after (0, $\tau(0)$) in a plot between $\tau(q)$ and q helps

to comment on the strength of the multifractal nature. The base width of the spectrum $f(\alpha)$ also reflects the strength of multifractal nature in the time series.

A wider singularity spectrum indicates a higher degree of multifractality, and a narrow width indicates lesser degree of multifractality. For a multifractal time series, the shape of singularity spectrum will be an inverted parabola whose left and right-hand wings correspond to positive and negative q, respectively. The width of the spectrum $f(\alpha)$ reflects the strength of multifractality. The shape and extent of the singularity spectrum $f(\alpha)$ curve contain significant information about the distribution characteristics of the examined data set and describe the singularity content of the time series. The degree of multifractality of a time series is characterized by the difference between the maximum and minimum values of α,$\Delta\alpha = \alpha_{max} - \alpha_{min}$ $\Delta\alpha = \alpha_{max} - \alpha_{min}$. This parameter is identical to the width of the singularity spectrum $f(\alpha)$ at $f = 0$. Asymmetric index (R) is a useful parameter for multifractal analysis. It is obtained by the following relation (Hou *et al*., 2017):

$$R = \frac{\Delta\alpha_L - \Delta\alpha_R}{\Delta\alpha_L + \Delta\alpha_R}, \tag{A4}$$

where $\Delta\alpha_L = \alpha_0 - \alpha_{min}$ and $\Delta\alpha_R = \alpha_{max} - \alpha_0$ are, respectively, the width of left- and right-hand branches of the multifractal spectrum curve; their values describe the distribution patterns of high and low fluctuations and α_0 is the singularity exponent for $q = 0$. The parameter α_0 delivers valuable information about the structure of the studied processes with a high value indicating that it is less correlated and possess fine structure (Krzyszczak *et al*., 2018). The value of R ranges from -1 to 1. It quantifies the deviations of the multifractal spectrum curve. $R > 0$ suggests a left-hand deviation of the multifractal spectrum, likely to have resulted from some degree of local high fluctuations; $R < 0$ suggests a right-hand deviation with local low fluctuations, and $R = 0$ represents a symmetrical multifractal spectrum.